J. Fluid Mech. (1997), *vol.* 332, *pp.* 71–104

The structure and development of a counter-rotating wing-tip vortex pair

By WILLIAM J. DEVENPORT, JEFFREY S. ZSOLDOS AND CHRISTINE M. VOGEL

Department of Aerospace and Ocean Engineering, Virginia Polytechnic Institute and State University, Blacksburg, VA 24061-0203, USA

(Received 9 February 1996 and in revised form 22 July 1996)

Experiments have been performed to examine the turbulence structure and development of a pair of counter-rotating wing-tip vortices. The vortices were generated by two rectangular NACA 0012 half wings placed tip to tip, separated by 0.25 chordlengths. Preliminary studies showed the vortices to be insensitive to the introduction of a probe and subject only to small wandering motions. Meaningful measurements could therefore be made using hot-wire probes. Three-component velocity measurements were made 10 and 30 chordlengths downstream of the wing leading edges for a chord Reynolds number of 260000.

At 10 chordlengths the vortex cores are laminar. True turbulence levels within them are low and vary little with radius. The turbulence that surrounds the cores is formed by the roll-up of and interaction of the wing wakes that spiral around them. This turbulence is stretched and organized but apparently not produced by the circulating mean velocity fields of the vortices.

At 30 chordlengths the vortex cores have become turbulent. True turbulence levels within them are larger and increase rapidly with radius. The turbulent region surrounding the cores has doubled in size and turbulence levels have not diminished, apparently being sustained by outward diffusion from the core regions. The distribution of the turbulence has also changed, the wake spirals having been replaced by a much more core-centred turbulence field.

This change in flow structure contrasts sharply with what is seen in the equivalent isolated tip vortex, produced when one of the wings is removed. Here the vortex core remains laminar and the turbulence surrounding it decays rapidly with downstream distance. This implies that the transition to turbulence in the cores of the vortex pair is stimulated by interaction between the vortices. Spectral measurements at 10 chordlengths suggest that short-wave instability may be the cause.

1. Introduction

Interactions between counter-rotating vortices generated by lifting surfaces are commonly seen in the far wakes of aircraft and marine vehicles. Perhaps the most well-known interaction is Crow (1970) or long-wave instability. Crow showed that the mutual induction of a pair of infinite line vortices of opposite sign makes them unstable to coupled sinusoidal disturbances along planes that lie at about 45° to that joining the vortices. There have been numerous observations of full-scale aircraft wakes (Scorer & Davenport 1970; Garodz 1971; Chevalier 1973; Tombach 1973) and laboratory-scale flows (Eliason, Gartshore & Parkinson 1975; Sarpkaya 1983; Sarpkaya & Daly 1987; Liu 1992; Thomas & Auerbach 1994) confirming Crow's theory. Crow instability is

usually cited as the primary mechanism causing the break-up and dissipation of a counter-rotating vortex pair. As the amplitude of Crow instability grows, it starts to become nonlinear. Ultimately, at low background turbulence levels, the vortex cores link together and a series of ring vortices is formed. At higher turbulence levels, vortex bursting may diffuse the cores before linking can occur (Tombach 1973; Liu 1992; Sarpkaya & Daly 1987).

Vortex pairs may also be susceptible to short-wave instability, analysed theoretically by Widnall, Bliss & Tsai (1974) among others. This bending-mode instability, also predicted to occur along 45° planes, may occur independently on either vortex filament. There have been several observations of short-wave instability on vortex rings (e.g. Sullivan, Widnall & Ezekiel 1973; Maxworthy 1972, 1974, 1977; Didden 1977), where they have been seen to cause transition to turbulence. Studies of temporally evolving vortex pairs (Thomas & Auerbach 1994; Locke, Hirsa & Rubin 1993) also provided evidence of this phenomenon, but at wavelengths longer than those predicted by Widnall *et al.* (1974). Evidence of short-wave instability forming on spatially developing vortex pairs (such as those generated in the wake of an aircraft) is much rarer. Structures that may interact with this instability are visible in the contrail pictures of Scorer & Davenport (1970) and in the delta-wing wake flow visualizations of Miller & Williamson (1995) and Follin (1996). All show the formation of regular structures at wavelengths too small to be accounted for by Crow instability.

Inviscid instabilities and their consequences are, of course, only part of the interaction between the vortices. Interaction between their turbulence and mean-flow fields are also likely to be significant, especially when the ratio of core radius to vortex separation is significant. Quantitative turbulence measurements on interacting trailing vortex pairs are rare, however, and there appear to have been no studies in which the full cross-sectional structure of such a flow has been examined in any significant detail. Surveys of the near-wakes of lifting wings (El-Ramly & Rainbird 1977; McCormick, Tangler & Sherrieb 1968; Devenport *et al.* 1996), where counter-rotating vortex interactions are insignificant, suggest that this structure may be fairly complex because of the spiral wakes that surround and connect the vortex cores. Observations of vortex rings (e.g. Maxworthy 1974) suggest that complex turbulence structure may also be generated by the cores themselves.

Measurements have been made of core velocity profiles in the far wakes of aircraft and wind-tunnel models (e.g. McCormick *et al.* 1968; Ciffone & Orloff 1974, 1975, 1976; Burnham, Sullivan & Wilks 1976; Wilson *et al.* 1979; Corsiglia, Schwind & Chigier 1973). An observation made in several of these studies is that the cores appear to undergo a two-stage decay. Over the first 20 or more spanlengths downstream of the generating wing the cores appear not to grow and their strength remains constant (Ciffone 1974; Iversen 1976), this is referred to as the plateau region. Decay then begins, the peak tangential velocity falling as the inverse square root of streamwise distance. Iversen attributes this behaviour to the action of a non-equilibrium turbulence structure, on the basis of earlier turbulence model calculations by Donaldson (1972) and Baldwin, Chigier & Sheaffer (1973). However, because of the large streamwise distance before decay begins, interaction between the vortices also seems a strong possibility.

The object of our research is to provide some of the missing understanding of tip vortex flows, particularly of their turbulence structure. In a companion paper (Devenport *et al.* 1996, hereinafter referred to as DRLF) measurements made in the single tip vortex formed downstream of an unswept rectangular NACA 0012 half-wing were presented. Such a flow is a model of the early development of an aircraft wake,

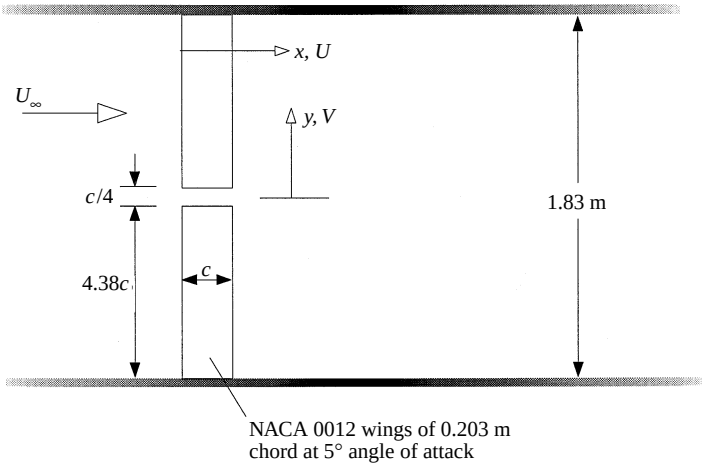

FIGURE 1. Schematic of the wind-tunnel test section showing the wing models and coordinate systems. Coordinate z is measured out of the paper from the quarter chord lines of the wings.

during which interaction between the tip vortices is negligible. DRLF found that this flow generates no turbulence of its own. Flow inside the core is laminar and the only turbulence outside the core is that associated with the unrolled-up part of the wake, which decays rapidly with streamwise distance. Velocity fluctuations in the core appear to be a consequence of inactive motion as the core is buffeted by this surrounding turbulence. These observations provide a plausible explanation of the plateau region seen in the early development of lifting wakes, since at flight Reynolds numbers laminar decay would be almost imperceptible.

In this paper we present turbulence measurements made in a pair of counter-rotating trailing vortices. These observations are more relevant to the later development of lifting wakes where interaction between the vortices is significant. The vortex pair was produced using the same configuration used to produce the isolated vortex, but with a second half-wing added (figure 1). This allows, to some extent, the single vortex study of DRLF to be used as a control, distinguishing effects associated with interactions between the vortex pair from those associated with individual vortex development.

This paper is organized as follows. First, we describe apparatus and instrumentation used to produce and measure the vortex pair (§2). Then the results and discussion are presented (§3), beginning with a description of the mean flow field and followed by a detailed analysis of the turbulence structure and its development with streamwise distance. Our principal conclusion (§4) is that there is a fundamental difference between the development of the vortex pair and that of the isolated vortex. Initially there are some similarities in structure: the vortex cores are laminar and the turbulence outside them is produced by the roll-up of the remainder of the wing wakes. Interaction between the vortices, however, causes the generation of new turbulence that penetrates the cores and substantially enhances the intensity and extent of the turbulent flow that surrounds them.

2. Apparatus and instrumentation

Most of the apparatus and instrumentation was identical to that described by DRLF. Measurements were taken in the Virginia Tech Stability Wind Tunnel which is a low-turbulence facility with a test section 1.83 m wide, 1.83 m high and 7.33 m

long. The vortex pair was generated using two identical half-wings mounted tip to tip (figure 1). Both had a rectangular planform, blunt tip, NACA 0012 section, chordlength c of 0.203 m and effective half-span of 0.879 m. The wings were mounted on opposite walls of the test section and positioned with their quarter chord lines collinear and perpendicular to the free stream. A tip separation of $0.25c$ was used and the angle of attack of both wings was fixed at 5°. Both wings were equipped with effective boundary-layer trips consisting of 0.5 mm diameter glass beads glued in a random pattern of average density 200 beads/cm^2 between the 20 and 40 % chord locations. A single hot wire was used to measure the properties of the resulting turbulence boundary layers at the wing trailing edges. Sample results are given in table 1.

Velocity and turbulence measurements were made using miniature 4-sensor hot-wire probes calibrated directly for flow angle. These probes sense the instantaneous velocity vector from within a 0.5 mm^3 measurement volume. Before using them it was necessary to demonstrate the absence of probe interference and to develop a method for dealing with the expected vortex wandering. These parts of the study are described in detail by DRLF. The absence of probe interference was demonstrated through flow visualizations, measurements with different probe configurations and theoretical estimates of the propagation of disturbances generated by the probe and the pressure field surrounding it. Vortex wandering, the slow side-to-side movement of a vortex, was found to be of small amplitude in the present flows. It was therefore possible to accurately measure its amplitude, determine the magnitude of its effects on measurements and correct for most of those effects using a theoretical approach. We regard this theory of wandering effects, developed and described in detail by DRLF, as the key to the present study. Without quantitative estimates of wandering effects it is difficult, if not impossible, to reliably interpret measurements made in tip vortices.

In short, this theory is based upon the observation that the mean velocity field measured in the presence of wandering is the convolution of the true field and the probability density function of vortex position in the crossflow plane $p(y, z)$. This convolution can be inverted by assuming an axisymmetric true mean-velocity field and a Gaussian p.d.f. of vortex position

$$p(y,z) = \frac{1}{2\pi\sigma_y\sigma_z(1-e^2)^{1/2}}\exp\left[\frac{-1}{2(1-e^2)}\left(\frac{z^2}{\sigma_z^2}+\frac{y^2}{\sigma_y^2}-\frac{2yz}{\sigma_y\sigma_z}\right)\right], \tag{1}$$

where σ_y, σ_z and e are the r.m.s. amplitudes of wandering in the y- and z-directions and the correlation coefficient, respectively. The inversion procedure requires, as input, a mean velocity profile measured through the vortex centre and the statistics of the cross-flow velocity fluctuations at the core centre generated by wandering. As output, it gives estimates of the true mean-velocity field, the wandering amplitudes (σ_y, σ_z and e) and the apparent turbulence stress fields produced by the wandering motions. DRLF implemented this procedure for measurements made in the isolated vortex and found that it produced acceptable results for r.m.s. wandering amplitudes up to about 40 % of the core radius. They were able to use the estimated turbulence stress fields to distinguish between regions where wandering contributions to the measured stresses were significant, and regions where they were not. DRLF found high-pass filtering to be the most effective method of eliminating wandering contributions to Reynolds stress measurements. These same techniques are employed here.

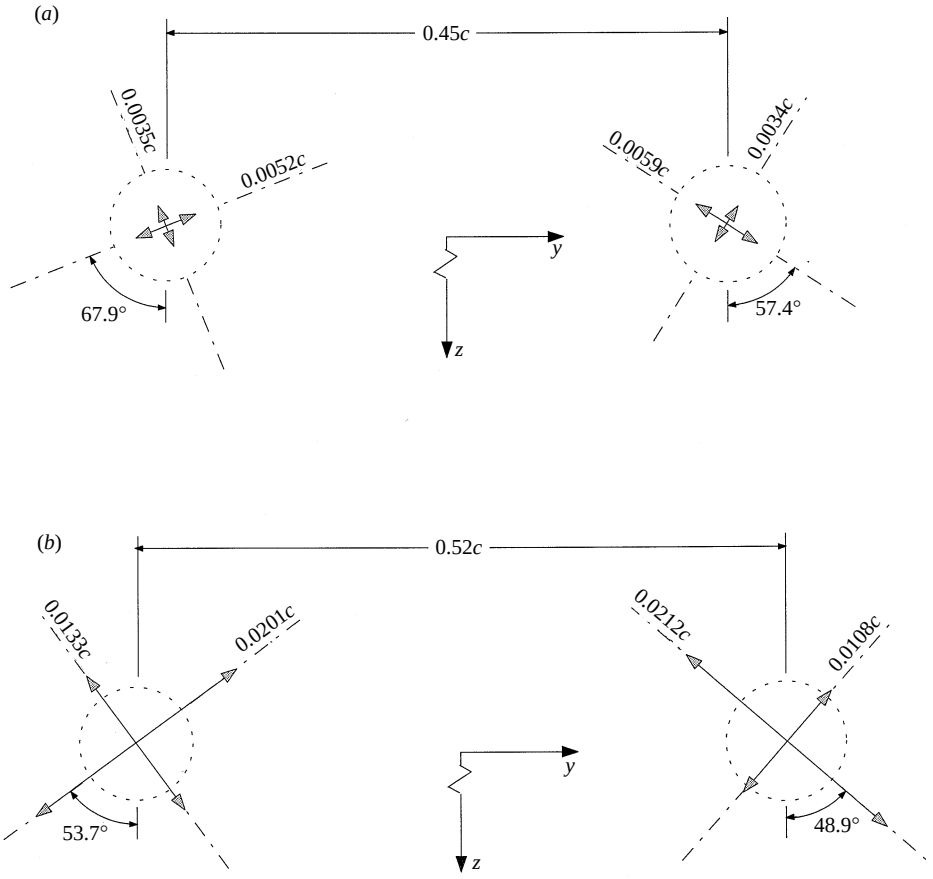

FIGURE 2. Scale diagram showing distance between vortices, core edges (dotted lines), and principal axes and r.m.s. of wandering amplitudes (arrows). Note that lengths of arrows are 10 times r.m.s. wandering amplitudes. (*a*) $x/c = 10$. (*b*) $x/c = 30$.

	δ/c	δ^*/c	Re_θ	
Pressure side $(+z)$	0.0336	0.0073	0.0042	980
Suction side $(-z)$	0.0584	0.0148	0.0078	1820

TABLE 1. Boundary-layer properties at the wing trailing-edge inferred from single hot-wire profiles measured 1 mm downstream at $y/c = 1.3$

3. Results and discussion

The free-stream aligned Cartesian coordinate system (x, y, z) (u, v, w) shown in figure 1 will be used to present most of the data. Many results are normalized on the wing chord c (0.203 m) and the free-stream velocity U_∞. Measurements were made at a chord Reynolds number $Re_c = U_\infty c/v$ of 260000, corresponding to a free-stream velocity of about 20 m s^{-1}. Typical uncertainties are listed in table 3 of DRLF.

Velocity measurements were made at $x/c = 10$ and 30 in cross-sectional planes through both vortex-core regions. Profiles were also measured through the wake of the positive y wing well inboard of its tip, at $y/c = 2.5$, where the flow was expected to be

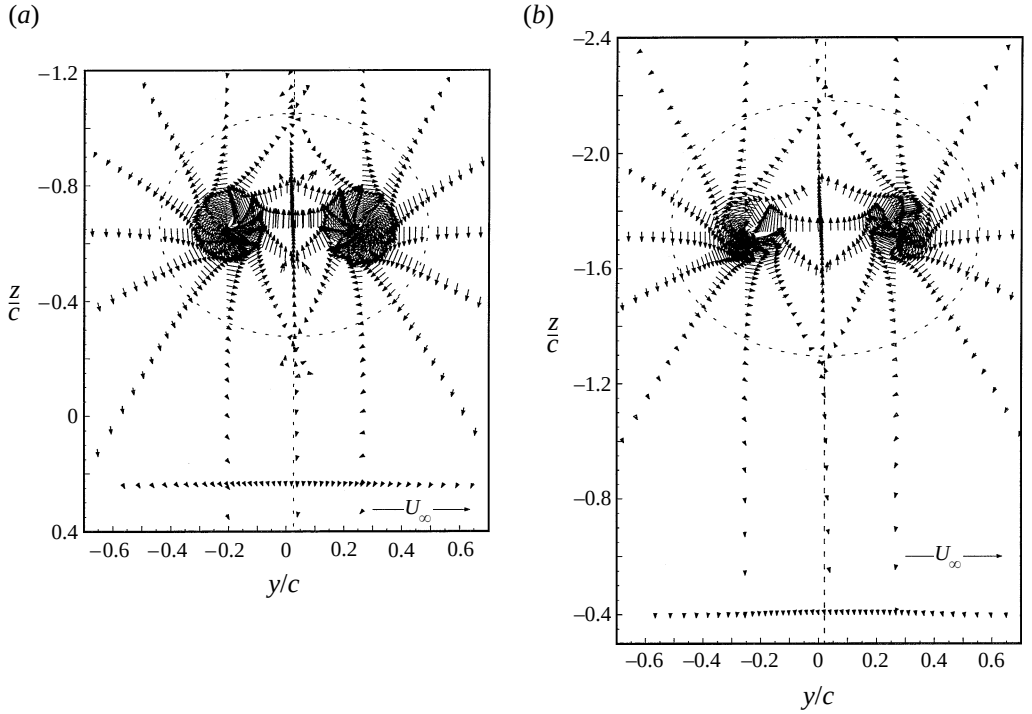

FIGURE 3. Mean cross-flow velocity vectors resolved in terms of velocity components perpendicular to the plane of the vortex cores. (*a*) $x/c = 10$. (*b*) $x/c = 30$. Dotted lines show Kelvin oval and stagnation streamlines estimated theoretically.

nearly two-dimensional. At each measurement point 614400 simultaneous samples of the three velocity components were recorded at a rate of 30 kHz (sufficient to calculate a detailed low-uncertainty spectrum) over a total sampling time of about 2 min.

Helium-bubble flow visualizations and velocity autospectra measured in the vortex cores showed both vortices to be subject to low-frequency wandering motions. Wandering amplitudes and directions, computed using DRLF's method, are illustrated in figure 2. At $x/c = 10$ the vortices have a strong preference for wandering motions along lines inclined at about $\pm 60°$ to the z-axis. Wandering amplitudes are about 0.6% c in these directions and about half that in the perpendicular directions. At $x/c = 30$ the wandering amplitudes are three to four times as big and the preferred direction of wandering is closer to $\pm 50°$. The symmetry of the wandering motions at both streamwise stations suggests they may be partially self-induced as well as the result of wind-tunnel flow direction unsteadiness (as proposed by DRLF). Since the wandering amplitudes were small compared to the core radii, DRLF's method could be used to correct mean velocity profiles and compute contributions of wandering to the measured turbulence stresses.

3.1. *Mean flow field*

Figures 3–5 illustrate the flow field in terms of mean cross-flow velocity vectors and contours of axial mean velocity and vorticity. Figure 5 shows the vortex core edges, defined as the loci of peak tangential velocity. Note that measurements were made with equal detail in both vortices, allowing one to judge the symmetry of the flow as well as the significance of some of the more subtle features of the results, based upon whether they appear on both sides of the centreline.

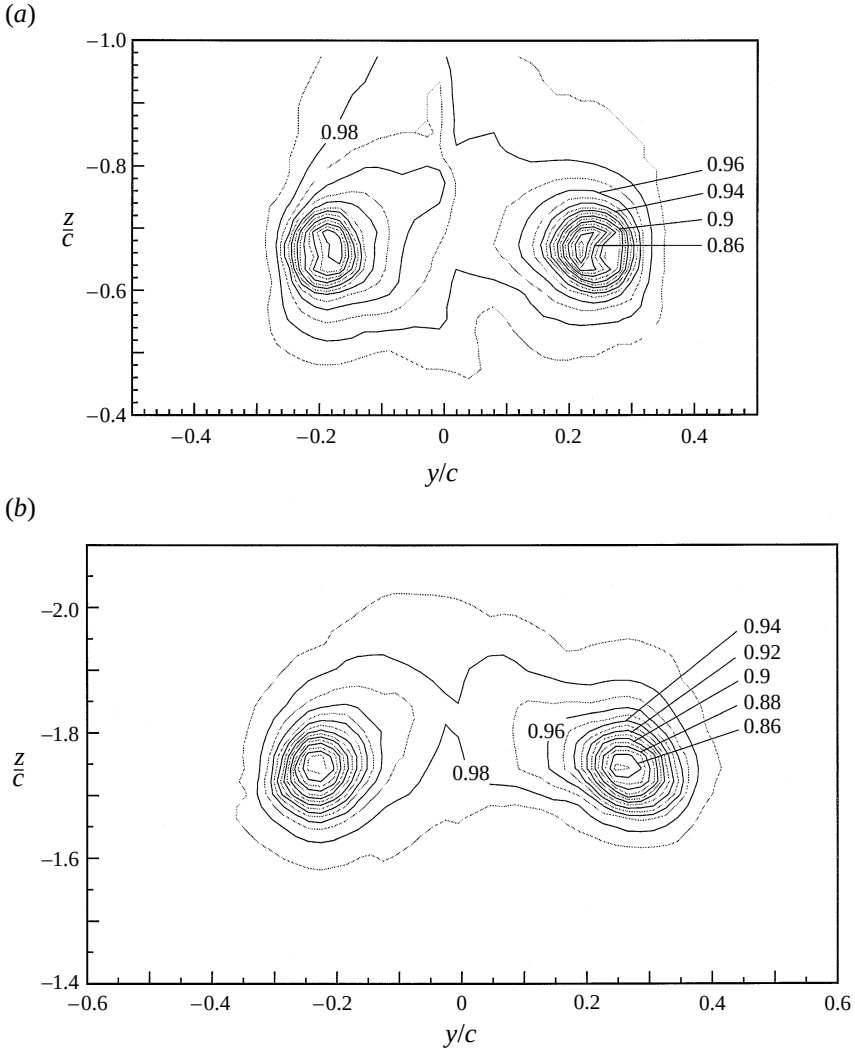

FIGURE 4. Contours of mean axial velocity U/U_∞. (*a*) $x/c = 10$. (*b*) $x/c = 30$.

Figures 3–5 show the vortices rising under their mutual induction from $z/c = -0.66$ at $x/c = 10$ to $z/c = -1.74$ at $x/c = 30$. The difference in the z-location of the vortex centres is less than $0.008c$ at both locations, indicating a matching of their strengths to within 0.5%. The vortex centres also move slowly apart from $0.45c$ at $x/c = 10$ to $0.52c$ at $x/c = 30$, the distance between them being approximately five core diameters at both stations. Some of this movement may be inviscid in nature. One expects the centroid of the vorticity distribution shed by each wing to remain approximately fixed during roll-up (Betz 1933). Since the centroids are inboard of the tips, the vortex cores initially move apart.

The circulating mean-velocity fields produced by the vortices (figure 3) appear quite similar at the two streamwise locations. Resolved in terms of velocity components perpendicular to the plane containing the vortex cores (as is done here), the vectors show two cross-flow stagnation points near $z/c = -0.2$ and -1.04, at $x/c = 10$ and $z/c = -1.25$ and -2.2 at $x/c = 30$. The mean axial velocity field shows substantial

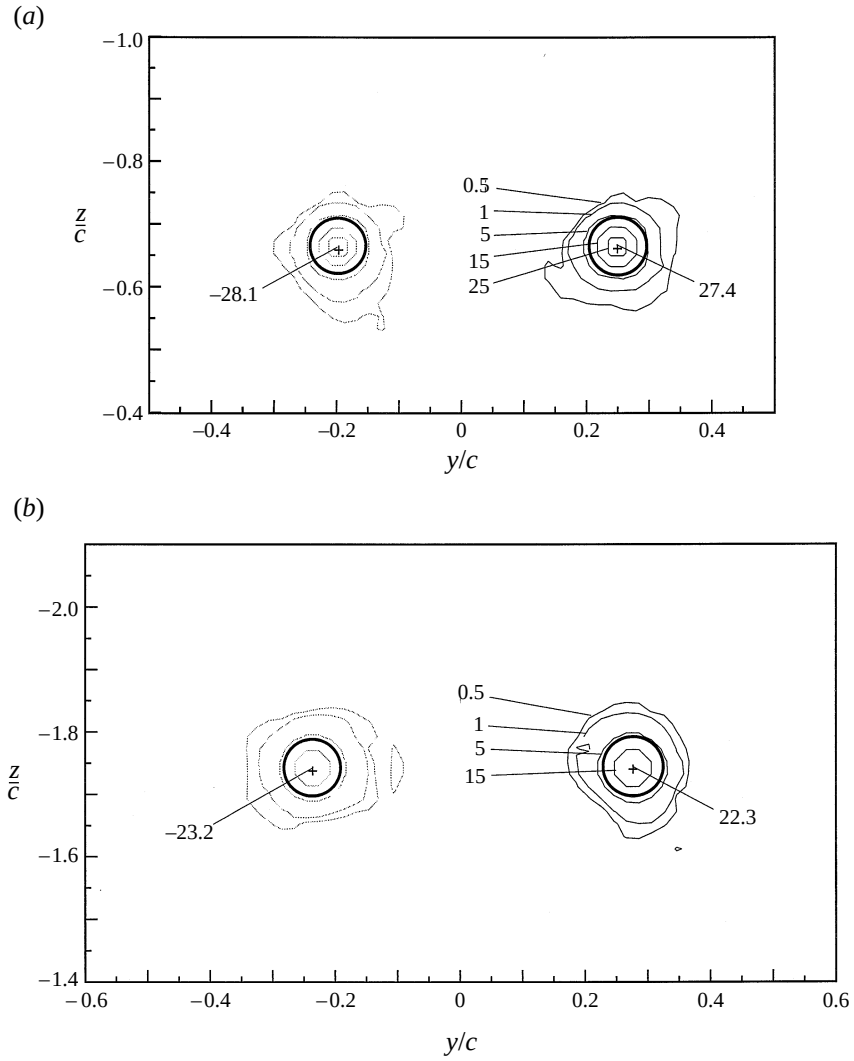

FIGURE 5. Contours of mean axial vorticity $\omega_x c/U_\infty$. (*a*) $x/c = 10$. (*b*) $x/c = 30$. Thick lines show core edges. Data in core regions corrected for wandering.

deficits in the core regions but only weak variations outside (greater than $0.08c$ from the vortex centres). The slightly lower axial velocities between the vortex cores are in part a consequence of the angle between the vortices and the x-axis. This causes a small proportion of the upwash to subtract from the U component.

The contours of figure 5 show almost all the vorticity to be concentrated in the vicinity of the cores. The concentrated vorticity fields are reflected in circulation distributions, plotted for each vortex as a function of radius r in figure 6. Circulation was computed by integrating along circular paths concentric with the vortex centres. For radii greater than half the vortex separation the circles were truncated by the plane of symmetry. At $x/c = 10$ the distributions are reasonably symmetric, given the mean-velocity uncertainty, and show about 50% of the theoretical root circulation Γ_0 to be contained within 1.2 core-radii of the vortex centres. (The root circulation was calculated assuming it to be the same as the circulation on a wing of infinite span, an

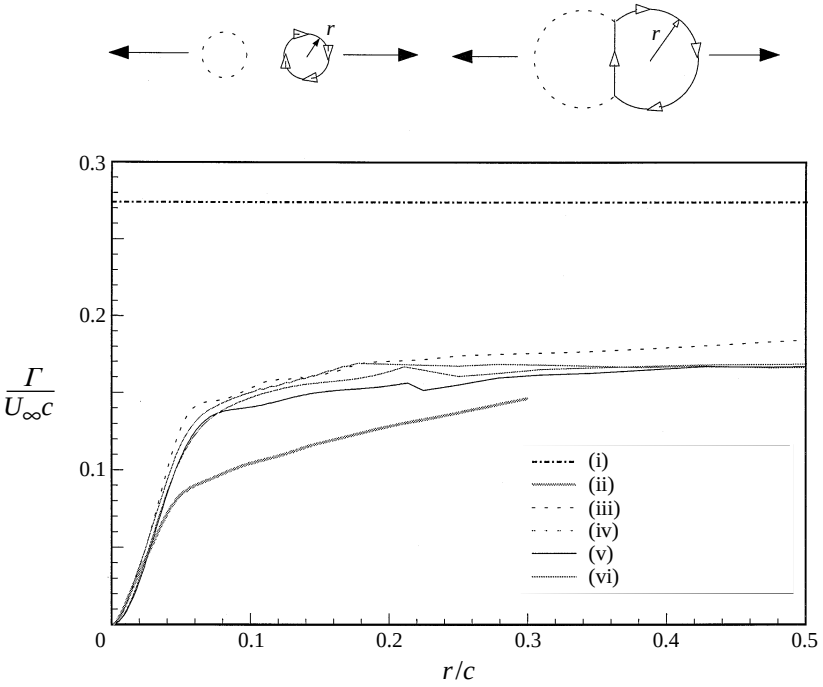

FIGURE 6. Circulation as a function of radius computed by path integration of the mean velocity measurements. For radii greater than half the vortex separation, circular paths were truncated as shown. Data in core regions corrected for wandering. (i) Root circulation; (ii) single vortex, DLRF; (iii) $x/c = 10$, right-hand vortex; (iv) $x/c = 10$, left-hand vortex; (v) $x/c = 30$, right-hand vortex; (vi) $x/c = 30$, left-hand vortex.

approximation that accounts for the combined effect of the two half-wings but ignores the gap separating their tips.) Outside this region the circulation increases only gradually with radius, becoming constant at about $0.6\Gamma_0$ at $r = 0.2c$. The remainder of the circulation is presumably contained in the un-rolled-up portions of the wing wakes left behind as the vortices rise under their mutual induction. At $x/c = 30$ the circulation distributions are almost unchanged.

Figure 6 also shows the circulation distribution of the single tip vortex (DRLF, case 2). The vortex pair shows a greater concentration of circulation in the core regions but a slower increase with radius outside. This is probably due to interference between the half-wings used to generate the pair. Interference would be expected to increase the root circulation (by about 14%) and cause a greater proportion of that circulation to be shed in the vicinity of the tips.

Since the flow outside the core regions is almost irrotational and free of substantial axial velocity gradients, a representative model can be constructed using a pair of two-dimensional point vortices, positioned at the vortex centres, and a uniform flow to counteract their drift. Such a model gives the total circulation in the vortices as a function of their rate of upward drift (i.e. from $z/c = -0.66$ to -1.74 in 20 chordlengths). This calculation gives $0.60\Gamma_0$ which is essentially equal to the value determined directly from the velocity measurements. The model also predicts stagnation points at $z/c = -0.27$ and -1.05 for $x/c = 10$ and $z/c = -1.29$ and -2.19 for $x/c = 30$ (close to the measured values) and the Kelvin oval streamline patterns illustrated in figure 3 (uncertainty and large point spacing prevent the determination

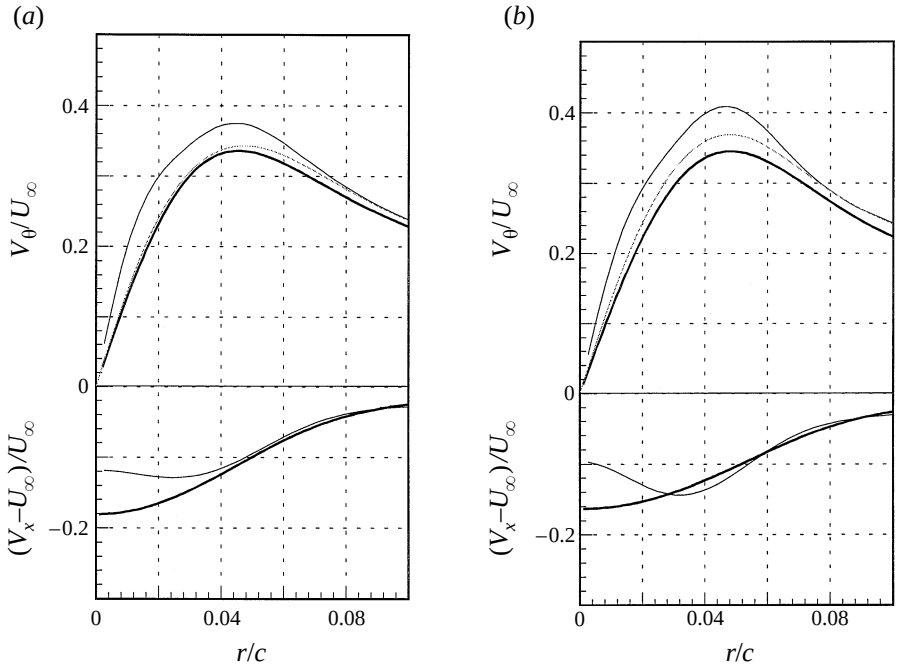

FIGURE 7. Circumferentially averaged profiles of the core aligned tangential and axial velocity components (v_θ and v_x) corrected for the smoothing effects of wandering; ..... show tangential profiles at $x/c = 30$ computed by assuming laminar decay from $x/c = 10$. (*a*) Left-hand, $(-y)$ vortex. (*b*) Right-hand $(+y)$ vortex. ——, $x/c = 10$; ——, $x/c = 30$, ..., $x/c = 30$ computed.

of these directly from measurements). While the streamline patterns appear reasonable they are unrealistic in one detail. With the vortices moving slowly apart the streamlines emanating from the upper stagnation point must fall slightly within those converging on the lower stagnation point, allowing for a slow entrainment into the Kelvin oval. This rate of entrainment can be characterized using Maxworthy's (1974) parameter $\Delta b/\Delta z$ (change in vortex spacing over vertical drift) which is 0.065 in this flow. (Note that the terms 'vertical' and 'horizontal' refer to directions parallel and perpendicular to the directions of lift, regardless of actual directions in the wind tunnel.) This is comparable to values quoted by Thomas & Auerbach (1994) for a temporally evolving vortex pair but, as noted by them, significantly larger than typical values for vortex rings (e.g. Maxworthy 1974, 1976). Such a comparison may be meaningless, however. Apart from the differences in geometry, vortex rings grow as diffusion transports vorticity out of the recirculation cell that surrounds them. As noted above, the growth in distance between the present vortices may also be a consequence of inviscid roll-up effects.

A total of 12 radial profiles were measured through each vortex core at both locations. The cores (figure 5) were found to be closely circular and axisymmetric, circumferential variations in the velocity being less than the uncertainty. Figure 7 shows circumferentially averaged profiles of the core aligned tangential and axial velocity components (V_θ and V_x) corrected for the smoothing effects of wandering. Corrections were $O(1\,\%)$ at $x/c = 10$ but $O(17\,\%)$ at $x/c = 30$ because of the increase in wandering amplitudes.

Despite the apparent equality of the overall vortex strengths, the mean flow structures of the cores differ significantly for $r/c < 0.08$. At $x/c = 10$ the core of the

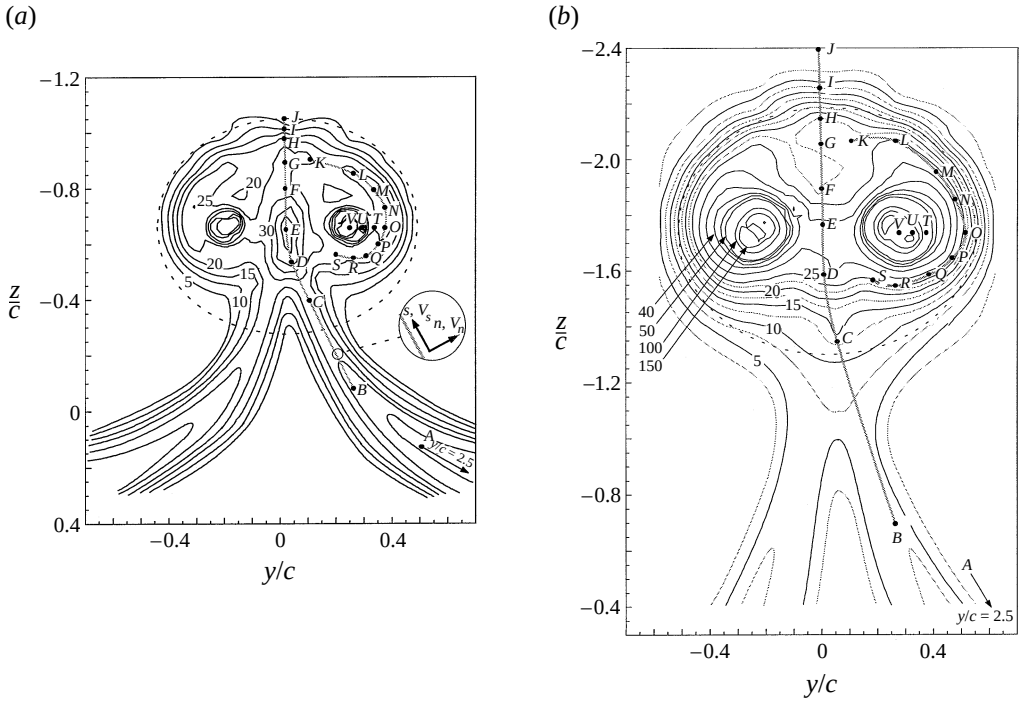

FIGURE 8. Contours of axial normal stress $\overline{u^2}/U_\infty^2$. (*a*) $x/c = 10$. (*b*) $x/c = 30$. Dotted lines show Kelvin oval. Contour levels multiplied by 10^5.

right-hand (positive y) vortex has a radius of $0.0465c$ and a peak tangential velocity of $0.409U_\infty$. The axial profile has a maximum at its centre superimposed upon a larger deficit, the net centreline deficit being 0.097% U_∞. The core of the left-hand (negative y) vortex has almost the same radius ($0.0446c$), but an 8% smaller peak tangential velocity ($0.375U_\infty$) and a less oscillatory axial profile. Since the generating wings were nominally identical these differences were not expected and may indicate a strong sensitivity to initial conditions. In retrospect, one might anticipate such sensitivity. Roll-up of the vortex from a blunt tip involves three-dimensional separation of the flow from salient edges. Studies of swept blunt flat-plate flows (Barkey Wolf 1987) have shown that such separations can be strongly influenced by microscopic imperfections in the edge.

At $x/c = 30$ the differences between the cores are smaller, presumably because of intervening decay. The core of the right-hand vortex has a radius of $0.0480c$, a peak tangential velocity of $0.345U_\infty$ and an axial velocity deficit of $0.163U_\infty$, the deficit profile having lost its central peak. These numbers are $0.456c$, $0.336U_\infty$ and $0.181U_\infty$ for the other core, the profile shapes being similar. The decay of the cores is also seen in the vorticity contours (figure 5) as the peak vorticity in both vortices falls from about $28U_\infty/c$ at $x/c = 10$ to near $23U_\infty/c$ at $x/c = 30$.

Figure 7 includes a calculation of the tangential velocity profiles at $x/c = 30$ assuming laminar cylindrical flow in each core ($V_r = 0$, $V_x \neq f(x)$) starting at the measured profiles at $x/c = 10$. The measured decay appears to be close to, but slightly greater than, that which would be expected from viscous effects alone.

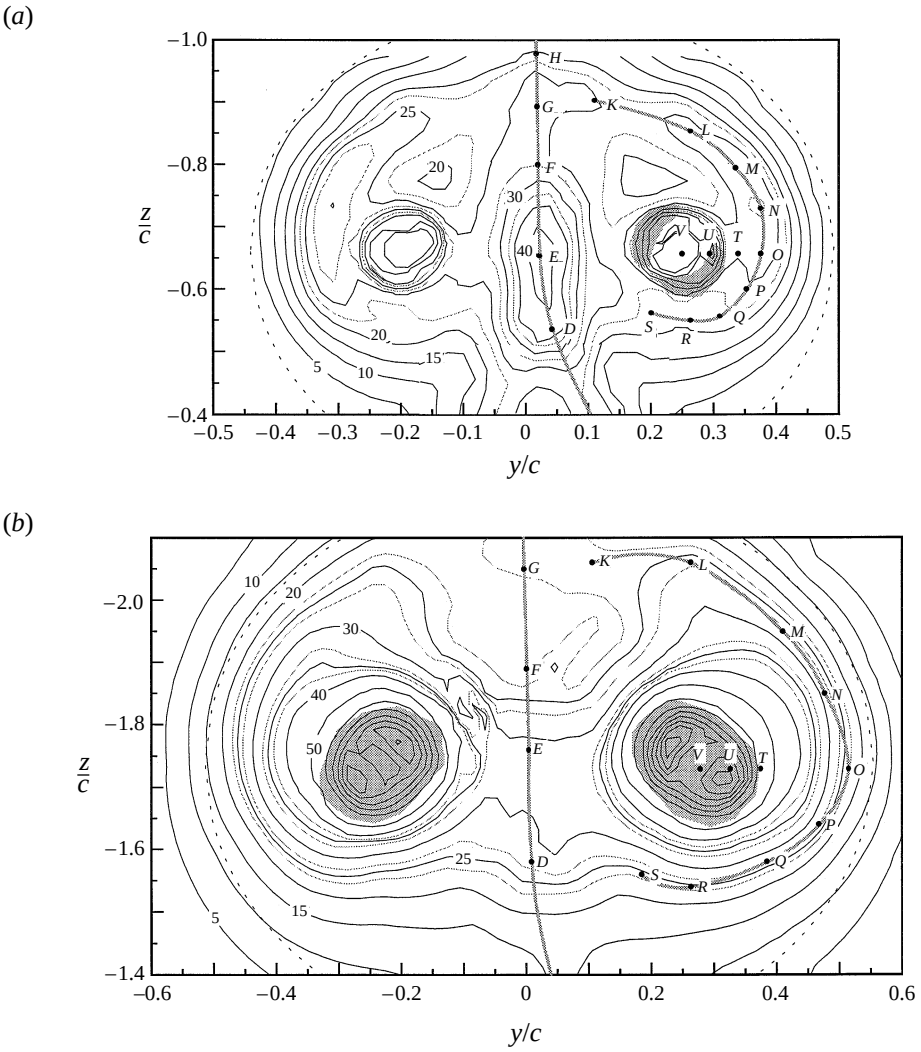

FIGURE 9. Contours of axial normal stress $\overline{u^2}/U_\infty^2$. (*a*) $x/c = 10$. (*b*) $x/c = 30$. Dotted lines show Kelvin oval. Grey regions indicate where wandering contribution is greater than 30 %. Contour levels multiplied by 10^5.

3.2. *Turbulence structure*

Figure 8 reveals the overall turbulence structure in terms of contours of axial normal stress $\overline{u^2}/U_\infty^2$. (As is common practice, we refer to the mean square velocity fluctuations and correlations as stresses, the multiplying density having been dropped for brevity.) Figures 9–11 show the structure surrounding the core regions in terms of contours of axial normal stress $\overline{u^2}/U_\infty^2$, cross-flow normal stress sum $(\overline{v^2}+\overline{w^2})/U_\infty^2$ and turbulence kinetic energy production (ignoring x derivatives), normalized on U_∞ and c. We plot $(\overline{v^2}+\overline{w^2})/U_\infty^2$ since this is invariant to rotation in the cross-flow plane. Figures 9–11 show shaded regions within which wandering is estimated to have contributed more than 30 % to the plotted turbulence quantity. (For comparison, 30 % is approximately the contribution that inactive motion makes to the streamwise normal stress in an attached turbulent boundary layer.) The bulk of turbulence stress measurements are free of substantial wandering effects. For $\overline{u^2}/U_\infty^2$ shading is almost absent at $x/c = 10$

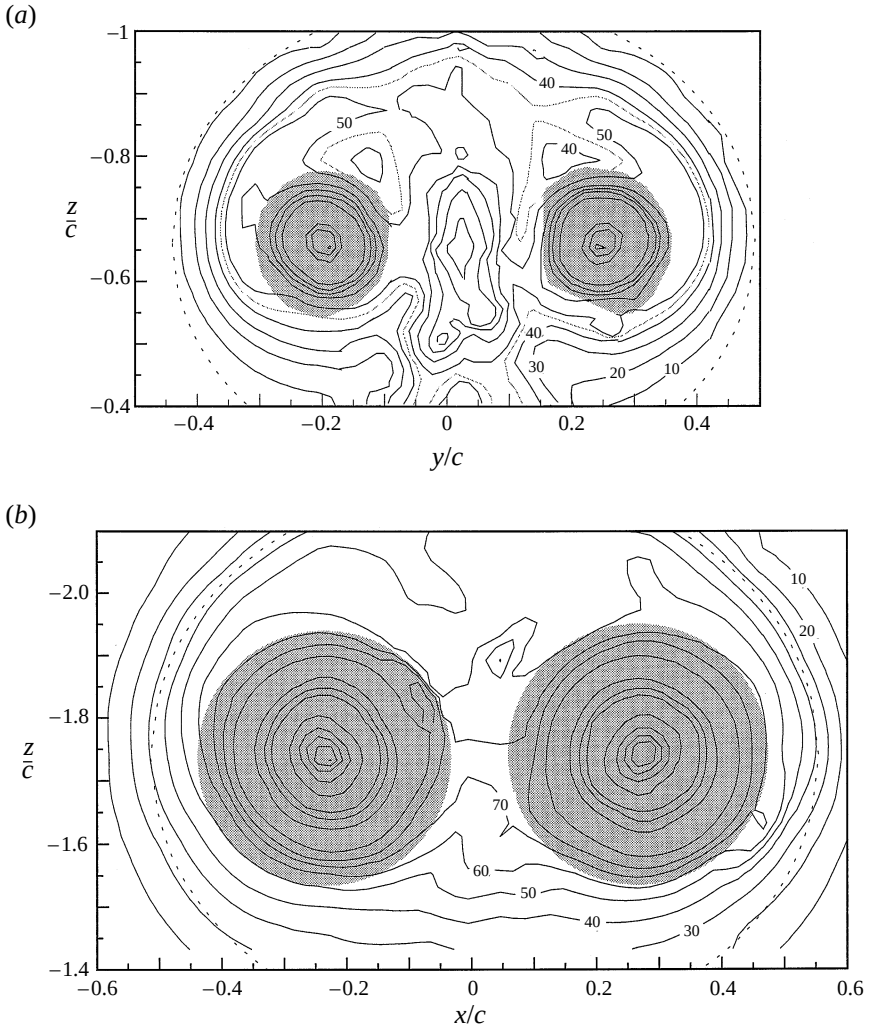

FIGURE 10. Contours of crossflow normal stress sum $(\overline{v^2}+\overline{w^2})/U_\infty^2$. (*a*) $x/c = 10$. (*b*) $x/c = 30$. Dotted lines show Kelvin oval. Grey regions indicate where wandering contribution is greater than 30%. Contour levels multiplied by 10^5.

and only covers the cores and their immediate vicinity at $x/c = 30$. For $(\overline{v^2}+\overline{w^2})/U_\infty^2$ and turbulent kinetic energy production the effects of wandering are greater, influencing turbulence stresses within about two core radii of the vortex centres and $x/c = 10$ and four radii at $x/c = 30$.

3.2.1. $x/c = 10$

At $x/c = 10$ the vortices are already joined in a single turbulent region, apparently formed by the roll-up of the two wing wakes. Unrolled-up sections of wake are clearly visible trailing below the vortices (figure 8*a*). Rolled-up sections appear as spiral shaped ridges in the contours of $\overline{u^2}/U_\infty^2$ and $(\overline{v^2}+\overline{w^2})/U_\infty^2$ that fill most of the Kelvin oval (figures 9*a* and 10*a*). In between the vortices there is a zone of relatively intense turbulence where the two wakes appear to have merged. Presumably the spiral sections of wake passed between the vortices before the merger was complete.

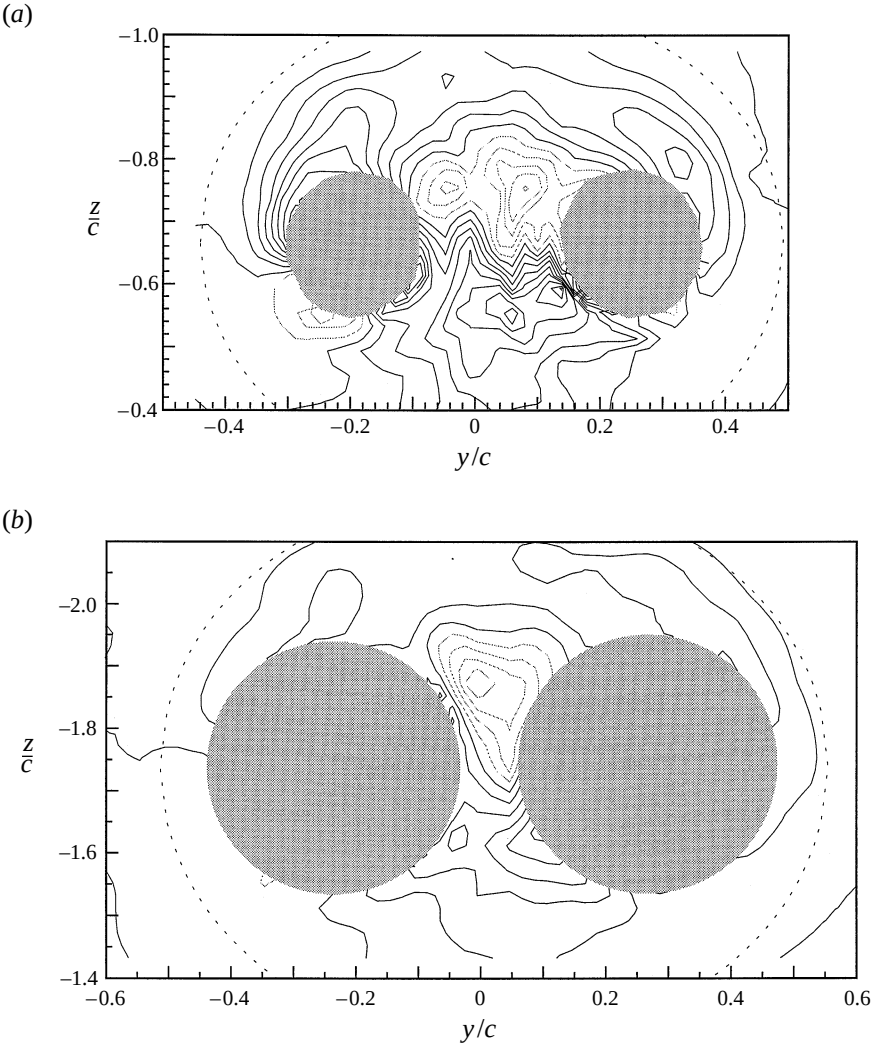

FIGURE 11. Contours of turbulence kinetic energy production (ignoring x derivates and normalized on U_∞ and c) in the core regions. (*a*) $x/c = 10$. (*b*) $x/c = 30$. Contour spacing 5×10^{-5}. Grey lines negative contours. Black lines zero and positive contours. Dotted lines show Kelvin oval. Grey regions indicate where wandering contributions are greater than 30%.

Surprisingly, the turbulence structure outside the core regions (greater than $0.08c$ from the vortex centres) has almost no visible counterpart in the mean flow field. The contours of mean axial vorticity and velocity (figures 4*a* and 5*a*) and the crossflow mean velocity vectors (figure 3*a*) show no discernable footprint of the rolled-up wakes. Axial mean velocity gradients, the primary source of instability and new turbulence in the unrolled-up sections of wake, are small and contribute little to the turbulent kinetic energy production over this entire region (figure 11*a*). Crossflow mean velocity gradients, a possible alternative source of new turbulence, are large but almost irrotational (figure 5*a*). It seems, therefore, that much of the turbulence rolled up outside the core regions may be passive, being redistributed and organized but no longer produced by the mean flow field. This does not mean that the flow is devoid of coherent instantaneous turbulence structure. Indeed, turbulence stress measurements

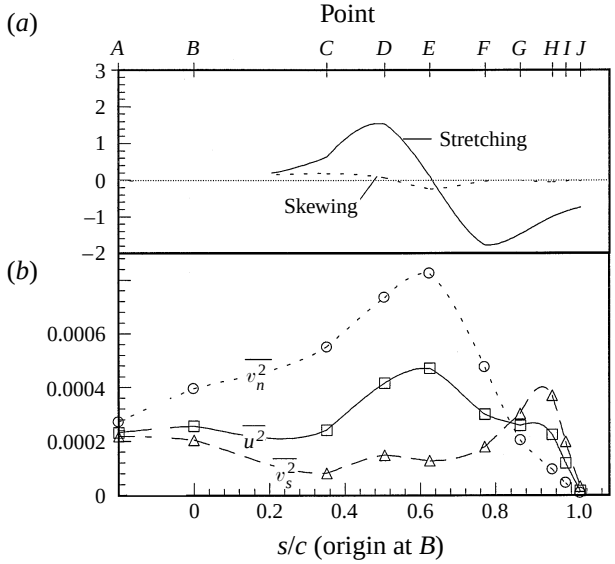

FIGURE 12. Flow properties at $x/c = 10$ at points A to J following the path shown in figure 8(*a*). (*a*) Mean rates of lateral stretching $\partial V_s/\partial s$ and skewing $\partial V_s/\partial n$ normalized on S_{2D}, the maximum axial mean-velocity gradient in the unrolled-up part of the wake (at A). (*b*) Turbulence normal stresses expressed in terms of velocity components parallel (v_s) and perpendicular (v_n, u) to the path.

and velocity spectra show ample evidence of large eddies apparently organized as they are stretched by the mean flow field.

Some of the evidence for these eddies may be seen by examining variations in flow properties along the two paths shown in figures 8*a* and 9*a*. The first, from points A to J, follows the centreline of the right-hand wake into the merger region between the vortices and then continues along the plane of symmetry through the top of the Kelvin oval. The second, from points K to S, follows the apparent centre of the right-hand spiral wake identified by the ridge in the $\overline{u^2}/U_\infty^2$ contours. Figures 12 and 14 show the turbulence normal stresses at these points expressed in terms of velocity components parallel (v_s) and perpendicular (v_n, u) to the paths. Figures 13 and 15 show autospectra of velocity fluctuations similarly resolved and plotted as $G_{UU}/U_\infty c$, $G_{V_s V_s}/U_\infty c$ and $G_{V_n V_n}/U_\infty c$ *vs.* fc/U_∞, where f is frequency in Hertz. The effects of the mean flow upon the turbulence are represented in figures 12 and 14 in terms of the mean rates of lateral stretching $\partial V_s/\partial s$ and skewing $\partial V_s/\partial n$, n and s being in the same directions as V_n and V_s (see figure 8*a*).

Between points A and C the unrolled-up wake is being stretched and thinned by the upward drift of the vortices. The minimum wake thickness, measured between the $\overline{u^2}/U_\infty^2 = 5 \times 10^{-5}$ contours, is about $0.2c$, compared at $0.33c$ at A furthest from the vortex cores. The axial velocity deficit also reduces from 5% at point A to around 1% at C. This reduction may occur because wake fluid cannot be convected into the Kelvin oval. The same unrolled-up sections of wake contained within it are thus continually stretched as the flow develops.

Stretching also influences the turbulence. Keffer (1965) observed lateral stretching of a two-dimensional wake to cause the intensification of eddies aligned with the stretching direction, the attenuation of other large-scale motions and an increase in the dissipation. These result in an increase in the intensity of velocity fluctuations perpendicular to the stretching direction and a reduction of those parallel. The

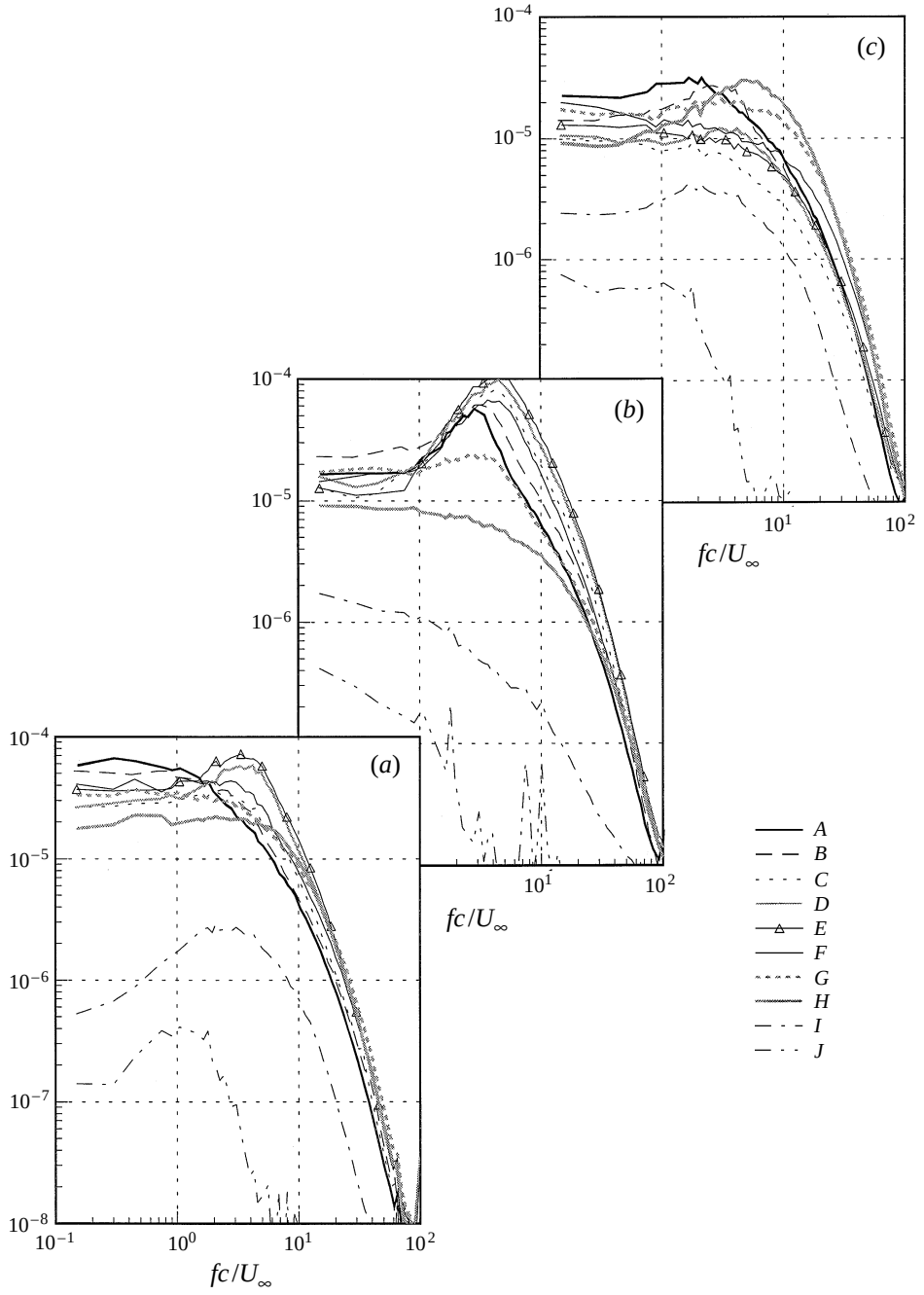

FIGURE 13. Velocity autospectra measured at $x/c = 10$ at points A to J following the path shown in figure 8(*a*) and expressed in terms of velocity components parallel (v_s) and perpendicular (v_n, u) to the path. (*a*) $G_{UU}/U_\infty c$. (*b*) $G_{V_nV_n}/U_\infty c$. (*c*) $G_{V_sV_s}/U_\infty c$.

turbulence stresses and velocity autospectra of the present flow both show precisely these effects (figures 12 and 13). Approaching the vortices from below, levels of $\overline{v_s^2}$ fall, and are three times smaller at C than at point A. The $G_{V_sV_s}$ spectrum shows most of this loss in energy occurring at low frequencies (figure 13*c*). By contrast $\overline{v_n^2}$ increases by a

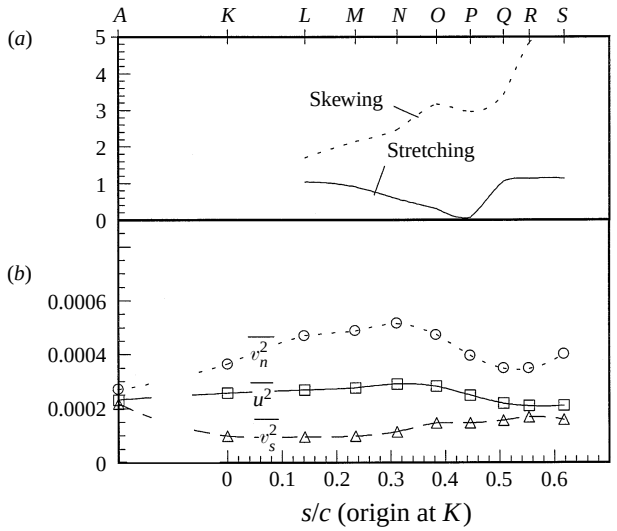

FIGURE 14. Flow properties at $x/c = 10$ at points K to S following the apparent centreline of the right-hand spiral wake (figure 8). (*a*) Mean rates of lateral stretching $\partial V_s/\partial_s$ and skewing $\partial V_s/\partial n$ normalized on S_{2D}, the maximum axial mean velocity gradient in the unrolled-up part of the wake (at A). (*b*) Turbulence normal stresses expressed in terms of velocity components parallel (v_s) and perpendicular (v_n, u) to the path.

factor of two. Most of this increase occurs at or above the preferred passage frequency of large eddies, identified by the peak in the $G_{V_nV_n}$ spectrum. This peak occurs near $fc/U_\infty = 3$ at A and B but jumps to near 4 at C, suggesting a typical eddy spacing of $\frac{1}{3}c$ to $\frac{1}{4}c$.

Moving between the vortex cores the two spiral wakes merge but many of the features of the turbulence structure here appear to have as much to do with intense stretching and compression of the turbulence by the mean flow field. Figure 12(*a*) shows the stretching rate reaching a maximum at D, just below the vortices, falling through zero at E and then to a negative minimum (a compression rate) at F just above the vortices. The stretching and then compression of the wake produces large increases in $\overline{v_n^2}$ and $\overline{u^2}$ and then sudden decreases. The resulting maxima are clearly visible in the turbulence stress contours of figures 9(*a*) and 10(*a*). In contrast, $\overline{v_s^2}$ remains low and almost constant in this region leading to considerable anisotropy of the turbulence (e.g. figure 12*b*, point E). This anisotropy is felt in the turbulence production (figure 11*a*), which is strongly positive below the line joining the vortex centres ($z/c = -0.66$), but actually negative above. The production reverses sign because it is completely dominated by $(\overline{v_n^2} - \overline{v_s^2})\,\partial V_s/\partial s$.

The anisotropy is consistent with a flow dominated by vertically aligned large eddies. Evidence for such is also seen in the spectra, particularly $G_{V_nV_n}$, which show a clear peak centred near $fc/U_\infty = 5$ (60% greater than the large-structure passage frequency at A). A lesser peak is also visible in G_{UU} spectra measured at points D and E. $G_{V_sV_s}$ spectra show no such feature, as might be expected. It is worth noting that these eddies may have had a quite different origin to those found in the unrolled-up sections of wake. Intense stretching in vortical flows can, by itself, organize large eddies out of otherwise incoherent turbulence (e.g. Melander & Hussain 1991).

The turbulence that exits the merging region is propelled upward towards the stagnation point at the top of the Kelvin oval. Vertically aligned eddies continue to be

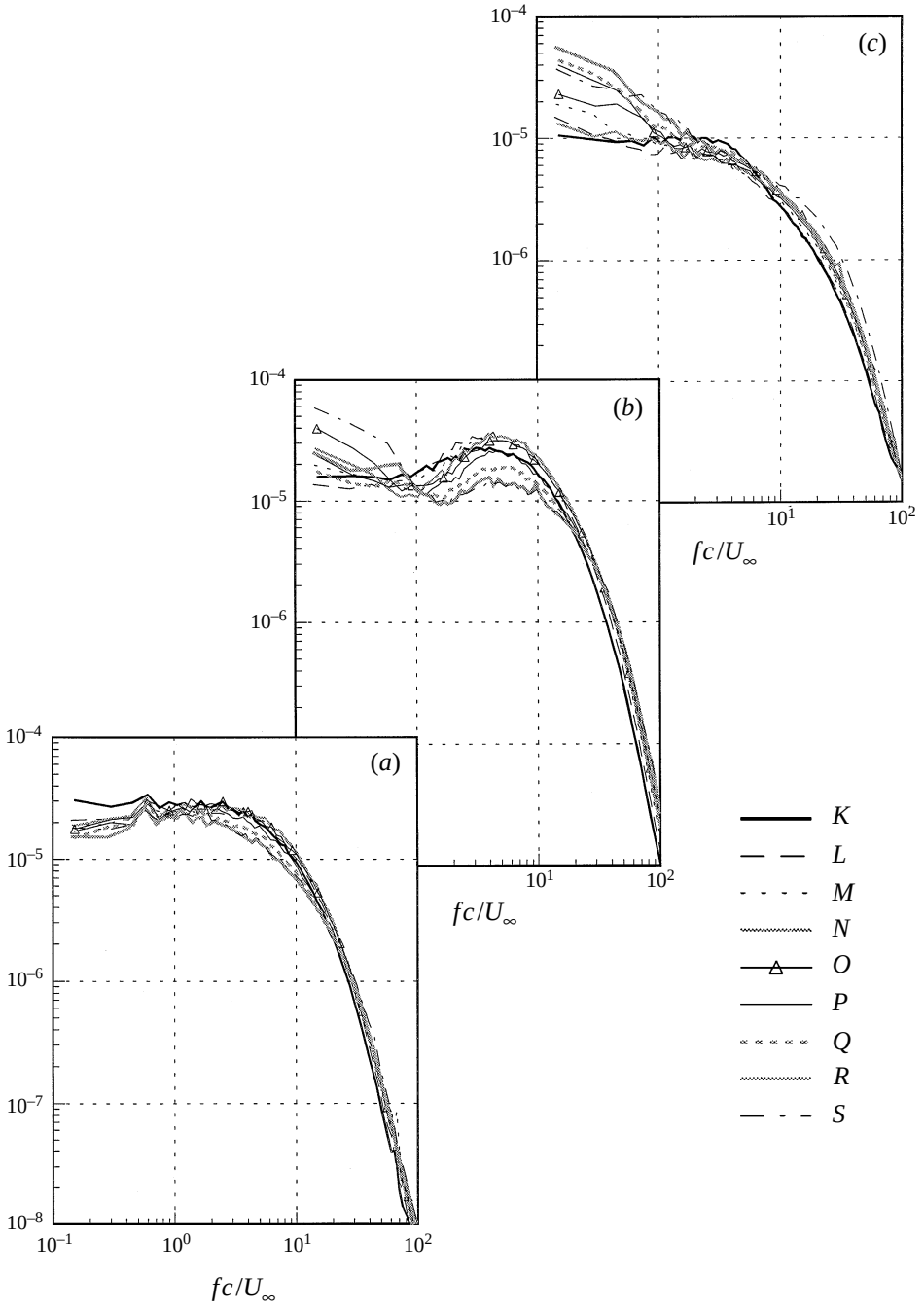

FIGURE 15. Velocity autospectra measured at $x/c = 10$ at points K to S following the apparent centreline of the right-hand spiral wake (figure 8*a*) and expressed in terms of velocity components parallel (v_s) and perpendicular (v_n, u) to the path. (*a*) $G_{UU}/U_\infty c$. (*b*) $G_{V_nV_n}/U_\infty c$. (*c*) $G_{V_sV_s}/U_\infty c$.

compressed in this region (figure 12*a*). Continuity, however, requires that the negative $\partial V_s/\partial s$ stretching rate here be balanced by an equal positive $\partial V_n/\partial n$ rate that tends to intensify and organize any remaining horizontally aligned turbulence. The action of these strain rates produces a reversal in the anisotropy of the stresses, $\overline{v_s^2}$ becoming

much larger than $\overline{v_n^2}$ and reaching a maximum near point H at $z/c = -0.98$. The reversal causes the turbulence production to become positive again at $z/c = -0.86$ (figure 11*a*). Turbulence spectra in this region (points *F*–*H*) show the disappearance of the peak in the $G_{V_nV_n}$ spectrum around $fc/U_\infty = 5$ and the appearance of a similar peak in $G_{V_sV_s}$. All these features suggest a change in the preferred orientation of the large eddies from vertical to horizontal. That these features are seen on the plane of symmetry suggests that there may be some linking of these eddies across the top of the Kelvin oval.

Continuing upward, we reach the upper stagnation point of the Kelvin oval and the edge of the turbulent region (point *J*). G_{UU} spectra measured here (figure 13*a*) show a distinct peak near $fc/U_\infty = 1$. The origin of this fluctuation is unclear since its frequency seems to be too low for it to be associated with turbulent eddies and does not match the frequency of any expected vortex-pair instability. These instabilities are discussed further below.

We now turn our attention to the spiral section of wake that surrounds the right-hand vortex core (points *K* to *S*, figures 8*a*, 14 and 15). Peaks in the $G_{V_nV_n}$ spectra measured at these points (figure 15*b*) suggest the presence of large eddies roughly aligned with the wake centreline. The effects of the mean stretching on these eddies may be seen in the anisotropy of the stresses, the difference between $\overline{v_n^2}$ and $\overline{v_s^2}$ fluctuating down and up apparently in response to the stretching rate. Evidence for the effects of mean skewing may be apparent in the velocity spectra. In this near irrotational flow, one would expect skewing to cause the breakup of large eddies. Indeed, the near monotonic increase in this strain rate along the spiral appears to be associated with a decline in spectral levels around the peak in the $G_{V_nV_n}$ spectrum (at $fc/U_\infty = 5$). In contrast, the high-frequency end of the $G_{V_nV_n}$ spectrum and most of the G_{UU} and $G_{V_sV_s}$ spectra remain surprisingly constant. Similar invariance in spectra measured along the centreline of a spiral wake surrounding a single-tip vortex was observed by DRLF.

Analysis of the turbulent kinetic energy production on the spiral wake centrelines (figure 11*a*) shows that it is almost entirely dominated by cross-stream stresses and velocity gradients. More specifically, expressing the production in terms of V_s and V_n (components apparently aligned with the large eddies at most stations), we find that production related to stretching and normal stresses $(\overline{v_n^2} - \overline{v_s^2})\,\partial V_s/\partial s$ far outweighs that due to skewing and shear stresses $-\overline{v_n v_s}\,(\partial V_n/\partial s + \partial V_s/\partial n)$. The implication is that this is not production associated with turbulent mixing.

The ridges of $\overline{u^2}/U_\infty^2$ that mark the spiral wakes disappear from view some two to three core radii from the vortex centres (figure 9*a*). Inside this region the turbulence stresses rise steeply to maxima inside the cores. A large proportion of the rise in $(\overline{v^2} + \overline{w^2})/U_\infty^2$ is a consequence of wandering, as indicated by the shaded region in figure 10(*a*). Wandering, however, is not responsible for most of the increase in $\overline{u^2}/U_\infty^2$ (figure 9*a*). To reveal the source of these fluctuations and the nature of the turbulence structure in the core and its vicinity, it is necessary to examine velocity spectra and filtered Reynolds stress fields.

Figure 16 shows autospectra of V and W velocity component fluctuations $G_{VV}/U_\infty c$ and $G_{WW}/U_\infty c$ at points *O*, *T*, *U* and *V* (see figure 8*a*) from the spiral wake centreline to the core centre of the right-hand vortex. Although altered by the distortion suffered by the spiral wake, the spectra at *O* have a turbulent wake-like form. Moving into the vortex core (points *U* and *V*) spectral levels at very low frequencies $fc/U_\infty < 2$ rise dramatically as a consequence of the wandering motions. It seems possible that some of the these motions are Crow (1970) instability. To predict the frequency and growth rate of this instability requires an estimate of the cutoff distance d. For a Rankine

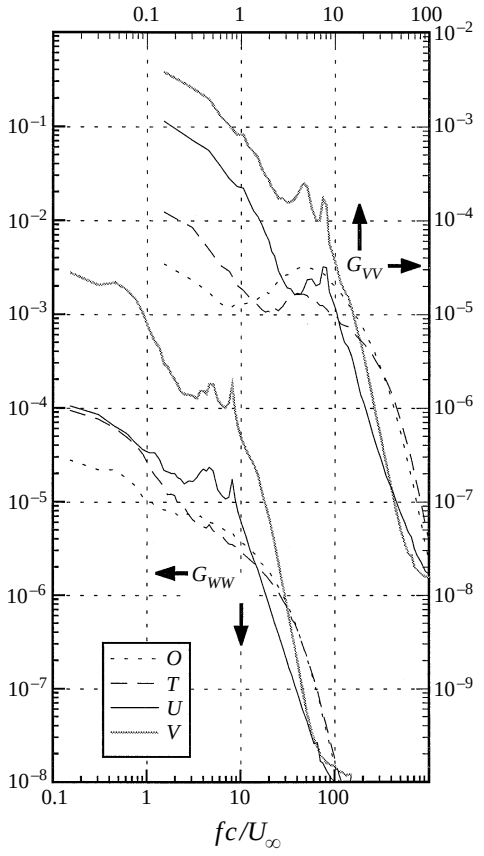

FIGURE 16. Autospectra $G_{VV}/U_\infty c$ and $G_{WW}/U_\infty c$ at points O, T, U and V (see figure 8*a*) from the spiral wake centreline to the core centre of the right-hand vortex at $x/c = 10$.

combined vortex, Crow gives $d = 0.321a$, where a is the radius of the vorticity-carrying core. For the present vortices we choose $a = 0.055c$, based upon the circulation profiles in figure 6 which show a distinct knee at this radius. This implies a most unstable wavelength of $3.4c$ that would grow by a factor e ($= 2.71828$) over a streamwise distance of $10.8c$. A $3.4c$ wavelength implies a frequency fc/U_∞ of 0.29. Spectral levels are strongly elevated around this frequency but the spectra show no distinct peak. This suggests that other sources of wandering may be important at this stage. One possibility, in additional to wind-tunnel unsteadiness, is that the wandering motions are generated indirectly by turbulent eddies in the spiral wake that surrounds each core. These eddies probably produce small random disturbances to the vortex core position. Like a random walk process, the disturbances would integrate along the length of the vortex to a net displacement that would increase with downstream distance. Because of the integrating effect, changes in the net displacement of the vortex at any given position would be of much lower frequency than the turbulence that generated them. Since the turbulence structure of the spiral wake is not axisymmetric, the wandering motions would have a preferred direction. Such a mechanism would be consistent with the symmetric nature of the wandering motions seen in figure 2 as well as the findings of DRLF.

While wandering dominates the low-frequency end of velocity spectra in the core, instabilities may be a factor at mid frequencies $2 < fc/U_\infty < 20$. Here the diffuse hump

in the G_{VV} spectrum, attributed to the passage of large eddies in the spiral wake, develops into two sharp peaks as the core is entered, at $fc/U_\infty = 4.9$ and 8.2. Similar peaks appear in G_{WW} and also in G_{VV} and G_{WW} in the opposite vortex core. Analysis of the VW cross-spectra at the core centres shows a significant coherence (> 0.3) between V and W velocity fluctuations around both peaks and a preferred direction of velocity fluctuations at the peak frequencies along planes inclined at around 45°. These features may indicate the presence of short-wave instability as analysed previously by Widnall *et al.* (1974) and others. According to Widnall *et al.* this instability should have a wavelength of about $2\pi a/\kappa$ where $\kappa \approx 2.5$. For the present vortices this is $0.138c$, which implies a frequency fc/U_∞ (seen by a stationary probe) of 7.2. Interestingly Maxworthy (1977) shows the development of short-wave instability on a vortex ring to be accompanied by the appearance of a second instability of about double the wavelength. A similar phenomenon could explain the presence of the lower-frequency peak seen here.

Observations of flow structures apparently produced by the latter stages of short-wave instability have been made in vortex pairs by Locke *et al.* (1993) and Thomas & Auerbach (1994). Locke *et al.* show the instability manifested in the formation of pairs of counter-rotating Taylor–Görtler type vortices around each vortex core spaced with an average wavelength of $0.37b$, where b is the distance between the vortex centres (neither of these authors measure core radii). Thomas & Auerbach's pictures appear to show similar structures but at an average spacing closer to $0.7b$. These wavelengths ($0.37b$ and $0.7b$) convected past a fixed probe in the present flow would produce frequencies fc/U_∞ of 6.0 and 3.2, respectively. Observation of other coherent motions that may interact with short-wave or other vortex instabilities have been made by Miller & Williamson (1995) and Follin (1996). They observe the formation of regular spanwise eddies that surround and connect the counter-rotating vortex pair in the wake shed from a lifting delta wing. The parts of these structures that surround the vortices grow in discrete jumps with distance downstream. At a chord Reynolds number of 285000 and a streamwise location some $20b$ downstream of the wing (equivalent to $x/c = 10$ in the present flow), Follin (1996) observes a discrete jump in the structure spacing from $0.25b$ to $0.4b$, approximately. Such spacing of turbulent structures in the present flow would produce frequencies of fc/U_∞ of eight and five, respectively, in surprising (but perhaps partly coincidental) agreement with figure 16.

At the high-frequency end of the spectrum $fc/U_\infty > 20$, where we would expect to see contributions from the smaller turbulent scales, spectral levels in both components fall by as much as an order of magnitude as the core is approached and entered. Bearing in mind the strong stabilizing effects of rotation, it is no surprise to see suppression of turbulence at the core centre (point V). However, it is a surprise to see it at the core edge (point U). The core edge is close to where the mean strain rate associated with the tangential velocity field reaches a maximum, where one might expect the production of turbulence from the rotational motion of the vortex to be at a maximum. The absence of small-scale turbulent fluctuations here suggests that such production may not take place and raises the possibility that, like the single vortex, the cores may be laminar.

A further clue to the nature of flow in the cores is found in the scaling of the velocity spectrum at the core centres. DRLF showed for the single-tip vortex that velocity fluctuations in the core centre scale not with core parameters, but with the length and velocity scales of the two-dimensional part of the wake far from the vortex core, L_w and U_W. This implies that the core is not producing turbulence (i.e. it is laminar) and that velocity fluctuations here are the result of inactive motions produced as the core is

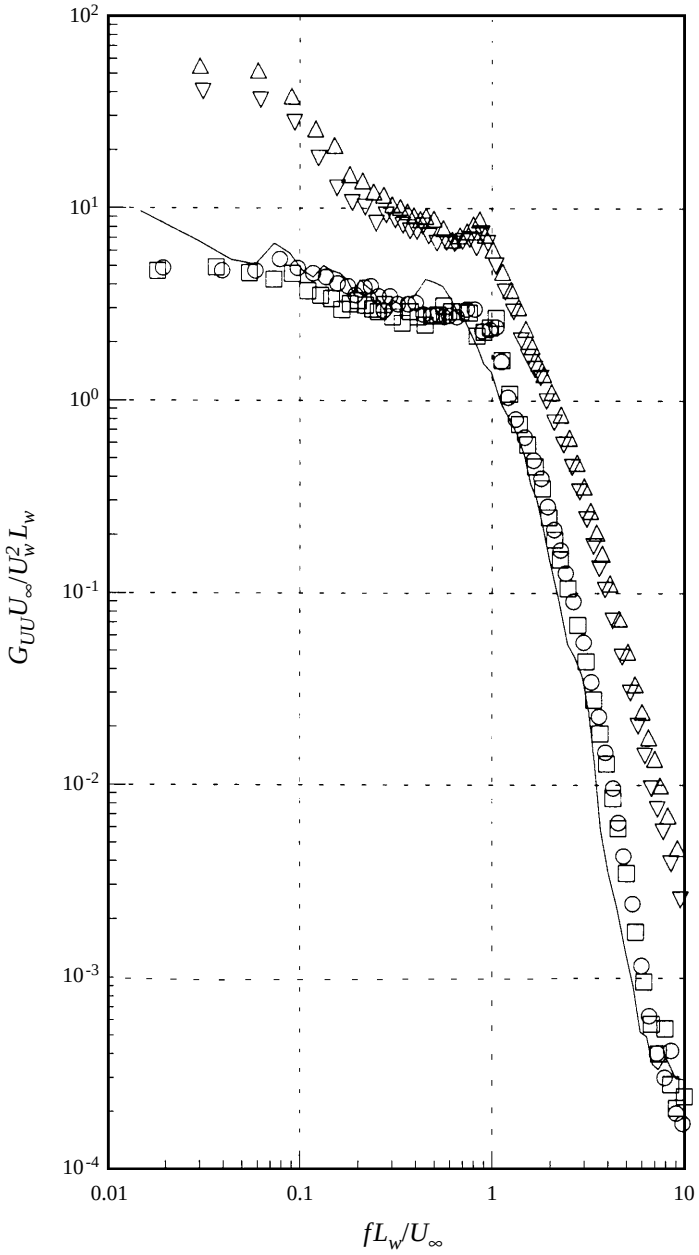

FIGURE 17. Comparison of core-centre U-component autospectra normalized on L_w and U_w, the length scales and velocity scales of the unrolled-up part of the wakes (at A). ——, Single vortex, DRLF case 8; ○, $x/c = 10$, right-hand core; □, $x/c = 10$, left-hand core; △, $x/c = 30$, right-hand core; ▽, $x/c = 30$, left-hand core.

buffeted by the surrounding spiral wake. Given that the present flow only differs from that studied by DRLF by the addition of a second vortex, we might expect a similar relationship to exist between core velocity fluctuations and wake scales, if the cores are laminar. Figure 17 shows core centre spectra measured in both vortices at $x/c = 10$, scaled on L_w and U_w and compared with one of DRLF's spectra measured in the centre of the single tip vortex at the same Reynolds number. (As done by DRLF, L_w

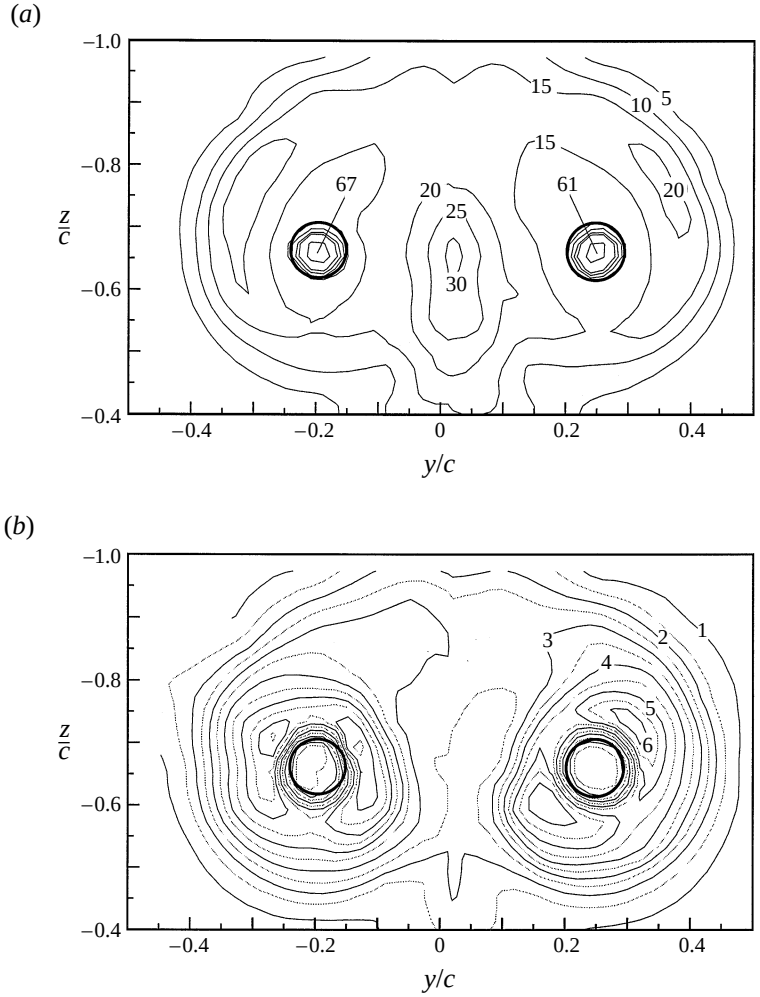

FIGURE 18. Contours of $\overline{u^2}/U_\infty^2$ at $x/c = 10$ high-pass filtered at frequencies of (*a*) $fc/U_\infty = 3$ and (*b*) 40. Contour levels multiplied by 10^5 in (*a*) and 10^6 in (*b*). Thick lines show core edges.

and U_w were determined from the $\overline{u^2}/U_\infty^2$ profile measured through the wake at $y/c = 2.5$.) Consistent with laminar core flows, the three spectra fall near the same curve. The collapse is not perfect, but much better than when normalized on any other parameters (i.e. core radius, peak tangential velocity, axial velocity deficit, free-stream velocity, chord) and well within the spread of single vortex data plotted by DRLF.

The true turbulence structure in the core regions can be illustrated for a broader range of positions by plotting filtered statistics. In figure 18 we plot contours of $\overline{u^2}/U_\infty^2$ high-pass filtered at frequencies of $fc/U_\infty = 3$ and 40, corresponding to lengthscales of $0.33c$ (7.3 core radii) and $0.025c$ (0.56 core radii), respectively. Filtering at $fc/U_\infty = 3$ (figure 18*a*) should eliminate almost all velocity fluctuations associated with wandering, but leave intact the bulk of fluctuations associated with coherent wake structures and core waves. The flow structure appears nearly identical to that shown by the conventional Reynolds averaged measurements (figure 9*a*) confirming that wandering was not an overwhelming contributor to $\overline{u^2}$ at this station. Filtering at $fc/U_\infty = 40$ (figures 18*b*) should eliminate all but the smaller turbulence scales. These contours

show no maximum in the wake merging region between the cores. This is expected since the stretching here should amplify the large eddies much more than the smaller-scale structures. In the cores these contours show fairly constant but very low stress levels, consistent with laminar flow. Outside the cores, stress levels increase reaching local maxima that sit on diagonally opposite sides of the core about 1.25 core radii outside its edge. DRLF attribute similar maxima, surrounding the core of their single vortex, to the final breakup and reorganization of wake turbulence by the core.

In summary, we find a number of similarities between the turbulence structure of the vortex pair at $x/c = 10$ and that of the single-tip vortex produced with one of the wings removed. Turbulence outside the core regions is associated mostly by the wing wakes as they are stretched and otherwise distorted by the mean flow. The vortex cores appear to be laminar, true turbulence levels within them are low and vary little with radius. Velocity fluctuations at the core centre scale on the length and velocity scales of the unrolled-up sections of the wake and not on core parameters. A comparison of figure 9(*a*) and figure 8(*d*) of DRLF shows the magnitude of the turbulence levels to be about the same in these two flow at $x/c = 10$.

There are also some important differences between these flows. In the vortex pair, roll-up of the wake spirals is limited to sections inside the Kelvin oval. The formation of these spirals is further limited by their merger between the vortices. Turbulence levels in this merging region are greatly amplified by stretching. In the stagnation region toward the top of the Kelvin oval there is evidence of new spanwise turbulence structures that may straddle the plane of symmetry. In the vortex cores sharp spectral peaks are seen, perhaps indicating the early stages of short-wave instability. All these features are absent in the single vortex flow.

3.2.2. $x/c = 30$

The turbulence structure of the flow surrounding the vortex cores at $x/c = 30$ is shown in figures 8(*b*), 9(*b*), 10(*b*) and 11(*b*). Below the vortices, the unrolled-up portions of the wing wakes are still visible but have barely grown in thickness, having been further stretched by the upward motion of the vortex pair. Turbulence stress levels here are slightly less than one-third of their values at $x/c = 10$, a factor of three decay would be expected in a two-dimensional wake. The elliptical turbulent region surrounding the cores has diffused well over the edge of the Kelvin oval. It covers roughly twice the area seen at $x/c = 10$ (area measured within the $\overline{u^2}/U_\infty^2 = 5 \times 10^{-5}$ contour) but turbulence levels within it are about the same. This remarkable lack of decay is in stark contrast to the turbulence stress field surrounding the single-tip vortex, which decays even faster than the unrolled-up part of the wake (compare figure 9 with figure 7 of DRLF).

The fact that the turbulence has spread but its intensity has not diminished suggests that new turbulence is being produced by the mean flow field. The instability and roll-up necessary for this production are only likely to occur where the flow is rotational, i.e. in the vicinity of the cores, and so the rest of the turbulence has presumably been diffused outward from the core regions. Consistent with this argument, the distribution of turbulence outside the core regions is quite different to that at $x/c = 10$, the wake spirals having been replaced by a much more core-centred turbulence field.

Despite the fact that the source of turbulence appears to have changed, part of the mechanism controlling the form of eddies outside the core regions, namely the stretching and straining of turbulence produced elsewhere, is the same as at $x/c = 10$. Consequently, some of the details of these structures appear unchanged. Consider, for example, the path (shown in figures 8*b* and 9*b*) that passes along the right-hand wing

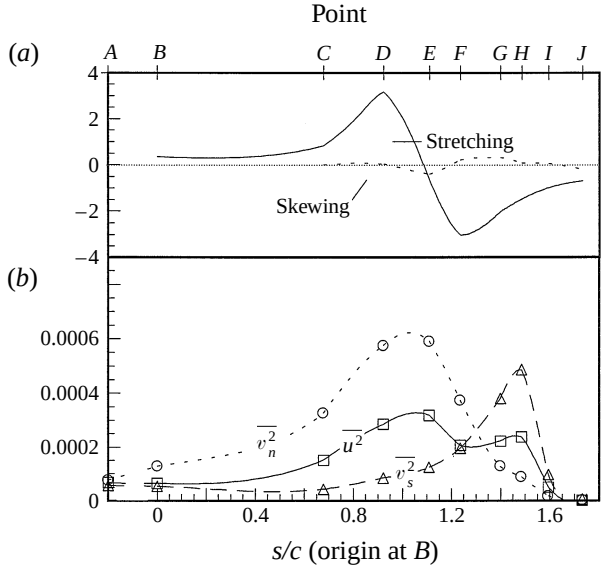

FIGURE 19. Flow properties at $x/c = 30$ at points A to J following the path shown in figure 8(*b*). (*a*) Mean rates of lateral stretching $\partial V_s/\partial_s$ and skewing $\partial V_s/\partial_n$ normalized on S_{2D}, the maximum axial mean-velocity gradient in the unrolled-up part of the wake (at A). (*b*) Turbulence normal stresses expressed in terms of velocity components parallel (v_s) and perpendicular (v_n, u) to the path.

wake, up between the vortex cores, and out through the top of the Kelvin oval. Figures 19 and 20 show turbulence stresses, mean strain rates and autospectra resolved into components parallel and normal to this path. In the unrolled-up wake (at B) the turbulence stresses and velocity spectra show the same features (increased anisotropy, an enhanced peak at the passage frequency of large structures) taken as symptomatic of lateral wake stretching at $x/c = 10$. The passage frequency of large-scale structures is about 1.7 (in terms of fc/U_∞) the decrease from three at $x/c = 10$ being roughly consistent with what would be expected of a two-dimensional wake. Stretching still dominates the region between the cores, reaching a maximum at D and falling to a negative minimum at F. The absolute stretching magnitudes are actually slightly less than at $x/c = 10$ but appear larger because of the decay in the normalizing parameters S_{2D} (the maximum axial velocity gradient in the unrolled-up wake at A). The anisotropy produced by the positive stretching is, if anything, greater than at $x/c = 10$ and is consistent with the presence of large-scale vertically aligned eddies. These eddies are visible as a strong peak in the $G_{V_nV_n}$ spectrum centred near $fc/U_\infty = 2.8$. Curiously, the ratio between this frequency and the passage frequency of large eddies in the unrolled-up wakes is almost the same as at $x/c = 10$. The anisotropy of the stresses and the reversal of the stretching rate again produces a region of negative turbulence production (figure 11*b*) located between $z/c = 1.72$ and 1.95 on the plane of symmetry.

Moving upward into the stagnation region, the continuing negative stretching in the vertical direction (by $\partial V_s/\partial s$) and the accompanying positive horizontal stretching (by $\partial V_n/\partial n$) produces a change in the apparent orientation of large-scale structures much like that seen upstream. The evidence includes a reversal of the anisotropy in the stresses ($\overline{v_s^2}$ becoming larger than $\overline{v_n^2}$ and reaching a maximum near point H ($z/c = -2.14$) and a shift of the spectral peak attributed to large eddies from $G_{V_nV_n}$ to $G_{V_sV_s}$. The maximum value of $\overline{v_s^2}$ is, in absolute terms, actually larger than

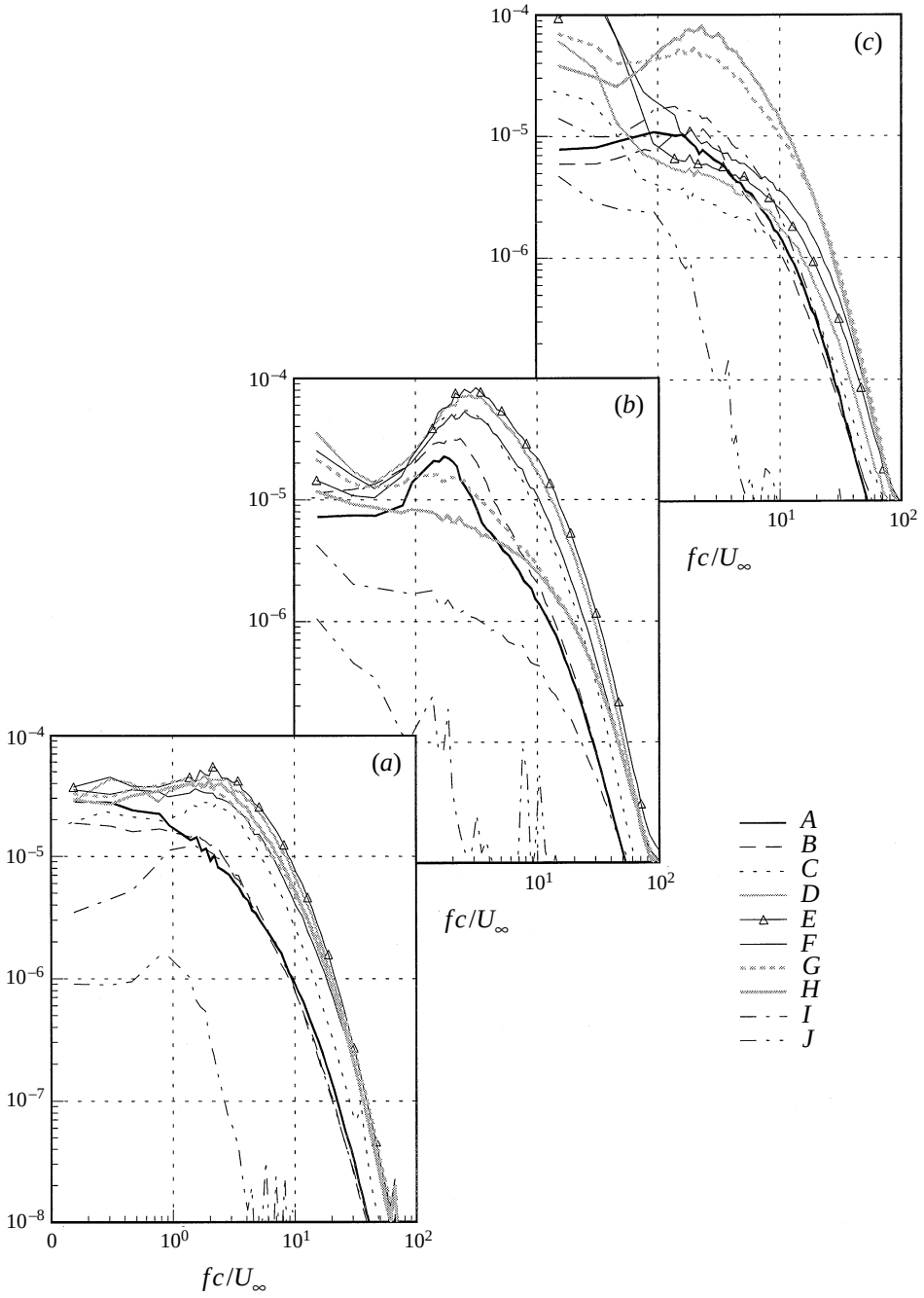

FIGURE 20. Velocity autospectra measured at $x/c = 30$ at points A to J following the path shown in figure 8(*b*) and expressed in terms of velocity components parallel (v_s) and perpendicular (v_n, u) to the path. (*a*) $G_{UU}/U_\infty c$. (*b*) $G_{V_nV_n}/U_\infty c$. (*c*) $G_{V_sV_s}/U_\infty c$.

at $x/c = 10$, underlining the lack of decay in turbulence levels. Again, we suspect that the horizontally aligned large eddies suggested by the results link the two sides of the Kelvin oval. G_{UU} spectra measured at the very top of the turbulent region (Point J) show, as at $x/c = 10$, a low-frequency peak at around $fc/U_\infty = 1$.

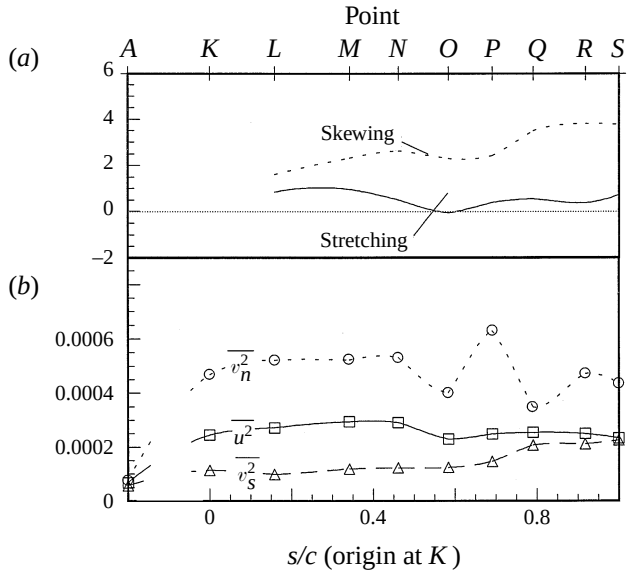

FIGURE 21. Flow properties at $x/c = 30$ at points K to S following the path shown in figure 8(*b*). (*a*) Mean rates of lateral stretching $\partial V_s/\partial s$ and skewing $\partial V_s/\partial n$ normalized on S_{2D}, the maximum axial mean-velocity gradient in the unrolled-up part of the wake (at A). (*b*) Turbulence normal stresses expressed in terms of velocity components parallel (v_s) and perpendicular (v_n, u) to the path.

Consider now the turbulent region surrounding the right-hand vortex. We have chosen to examine the flow properties along a path that follows the $\overline{u^2}/U_\infty^2 = 25 \times 10^{-5}$ contour, this turbulence level being roughly equal to that found on the spiral wake centreline at $x/c = 10$ (figures 8*b* and 9*b*). This path is also approximately a cross-flow streamline. Turbulence stresses and autospectra resolved into components parallel and normal to this path (figures 21 and 22) show some evidence of coherent turbulent structures roughly aligned with it, i.e. roughly tangential to the vortex core. Most notably the $G_{V_nV_n}$ spectra all show a peak at around $fc/U_\infty = 2.4$ whereas none is visible in $G_{V_sV_s}$ or G_{UU}. Moving clockwise (from K to S) around the vortex spectral levels in the vicinity of the peak in $G_{V_nV_n}$ decay monotonically. This could indicate that the large-scale eddies are becoming increasingly disorganized as they convect around the oval, perhaps by the skewing imposed by the mean velocity field (figure 21). Note that all $G_{V_nV_n}$ and $G_{V_sV_s}$ spectra show elevated spectral levels at frequencies $fc/U_\infty < 1$ as a consequence of the wandering motions.

Now we turn our attention to the regions in and around the cores which, as argued above, are implicated as the source of much of the turbulence seen at $x/c = 30$. The contours of $\overline{u^2}/U_\infty^2$ (figure 9*b*) show turbulence levels increasing as the cores are approached, to levels higher than those seen at any point at $x/c = 10$. Wandering, however, obscures all of the turbulence structure associated with the core itself. The true structure here may be revealed by looking at spectra and filtered stress fields. Figure 23 shows autospectra of V and W component spectra along the radial profile O, T, U, V that enters the core of the right-hand vortex. Moving toward the core (O to V) spectral levels at the lowest frequencies $fc/U_\infty < 1$ rise by more than two orders of magnitude as a consequence of the wandering. In contrast to $x/c = 10$ the wandering motions here appear to have a preferred frequency, since the G_{ww} spectrum develops a clear peak centred at $fc/U_\infty = 0.36$. This is fairly close to the frequency predicted for Crow instability of 0.29. (Note that using conditions at $x/c = 30$ for this prediction instead of $x/c = 10$ makes no significant difference to the results.) The

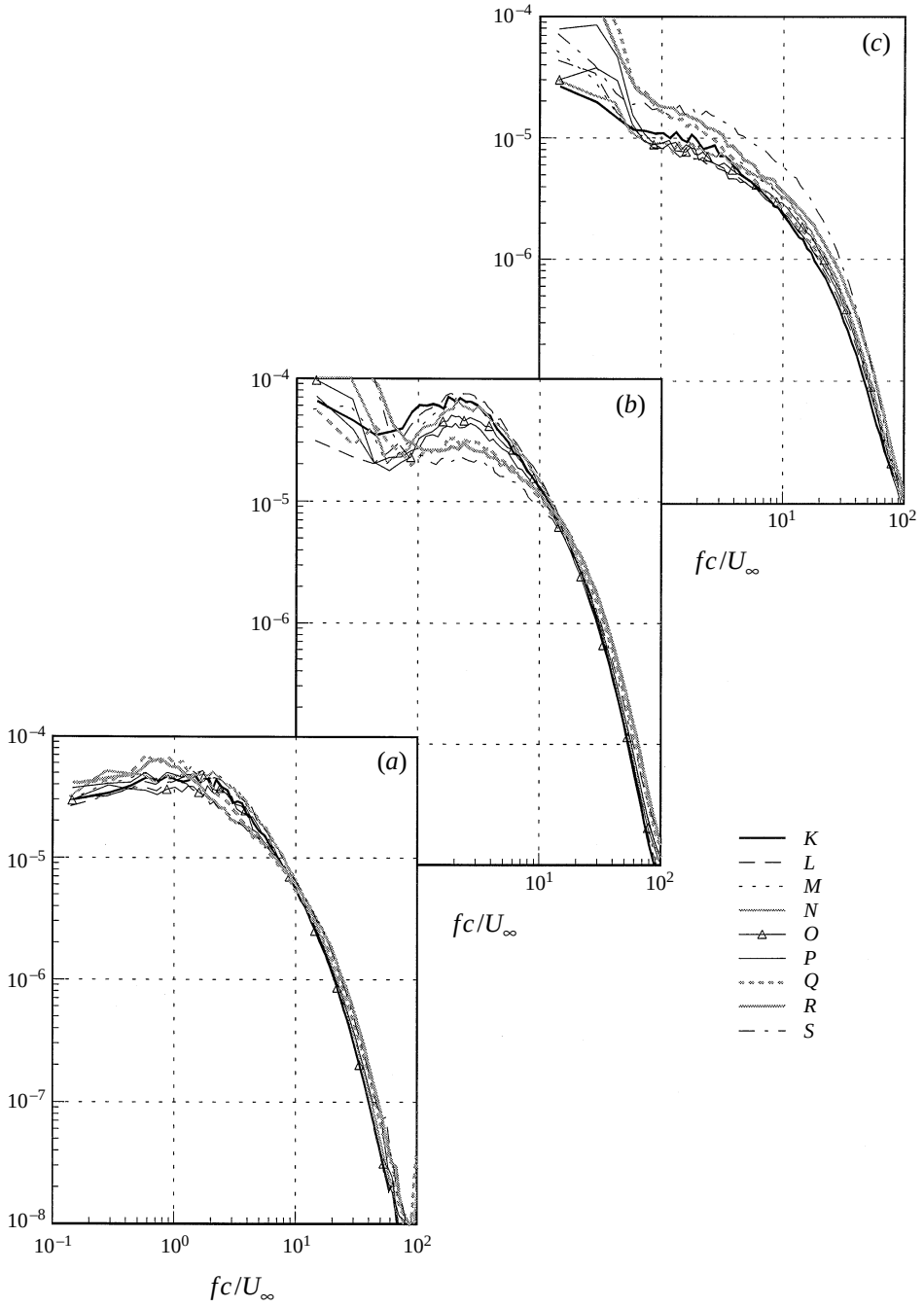

FIGURE 22. Velocity autospectra measured at $x/c = 30$ at points K to S following the path shown in figure 8(*b*) and expressed in terms of velocity components parallel (v_s) and perpendicular (v_n, u) to the path. (*a*) $G_{UU}/U_\infty c$. (*b*) $G_{V_nV_n}/U_\infty c$. (*c*) $G_{V_sV_s}/U_\infty c$.

direction of this dominant core motion is clearly shown by the double-peaked distributions of axial normal stress visible in both core regions (figure 9*b*). It is simple to show that these distributions are a consequence of oscillation of a near Gaussian axial velocity deficit along an axis coincident with a line joining the two peaks. These

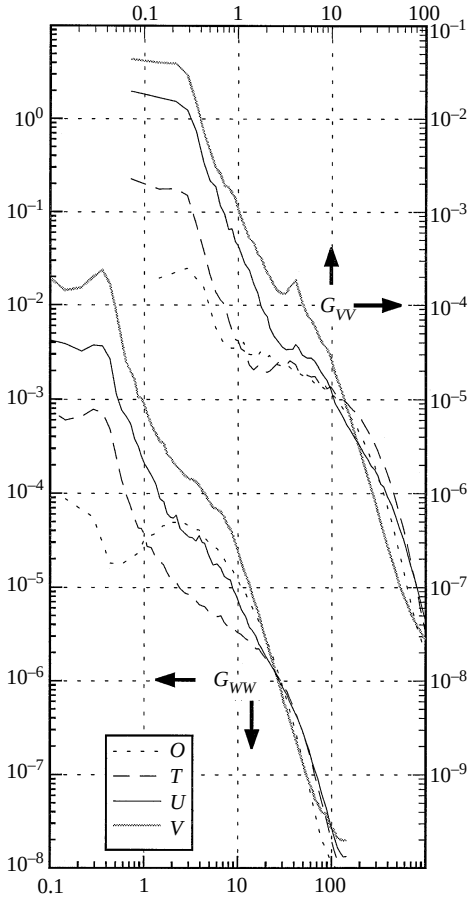

FIGURE 23. Autospectra $G_{VV}/U_\infty c$ and $G_{WW}/U_\infty c$ at points O, T, U and V (see figure 8*b*) from the spiral wake centreline to the core centre of the right-hand vortex at $x/c = 30$.

lines are seen to lie roughly along $\pm 45°$ planes consistent with Crow's prediction. Based upon the growth rate calculated at $x/c = 10$, we would expect the amplitude of Crow instability to grow by a factor of 6.4 between $x/c = 10$ and 30 and thus associated spectral levels to increase by $6.4^2 \approx 40$ times. In fact, the increase in G_{WW} around $fc/U_\infty = 0.3$ is about tenfold (compare figures 16 and 23). This explains why the spectra at $x/c = 10$ show no distinct peak associated with this instability, it being well buried in the surrounding spectrum.

In the middle-frequency range $2 < fc/U_\infty < 20$, the core centre spectra no longer show the sharp spikes seen at $x/c = 10$ and attributed to the early stages of instability. Here, only one, much more diffuse, peak is visible in G_{vv} centred at $fc/U_\infty = 4.5$. This is close to the location of the lower-frequency spike seen at $x/c = 10$.

At the high-frequency end of the spectrum $fc/U_\infty > 20$ spectral levels fall as the core centre is approached. However, the fall is much less than that seen at $x/c = 10$. In addition, high-frequency turbulent fluctuations at the core edge (point U) are not suppressed at all, in complete contrast to $x/c = 10$. This change in relative spectral levels is not observed in the equivalent isolated vortex (DRLF).

The change in core structure implied by the above results is also apparent in the filtered statistics. In figure 24 we plot contours of $\overline{u^2}/U_\infty^2$, high-pass filtered at frequencies of $fc/U_\infty = 3$ and 40. Removing stress contributions from Crow instability

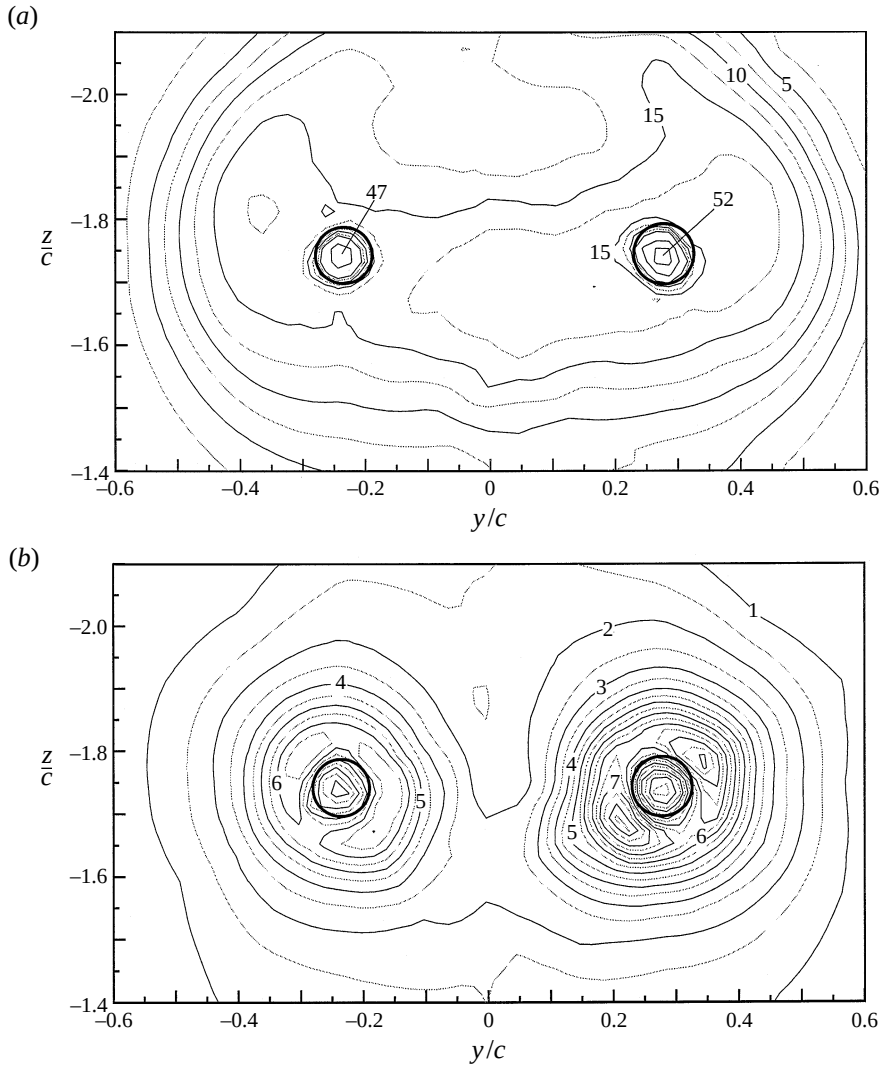

FIGURE 24. Contours of u^2/U_∞^2 at $x/c = 30$ high-pass filtered at frequencies of (*a*) $fc/U_\infty = 3$ and (*b*) 40. Contour levels multiplied by 10^5 in (*a*) and 10^6 in (*b*). Thick lines show core edges.

and other wandering by filtering at $fc/U_\infty = 3$ (figure 24*a*), makes little apparent difference to the turbulence structure (compare with figure 9*b*), except that it eliminates the double-peaked core stress distributions. Filtering at $fc/U_\infty = 40$ (figure 24*b*) reveals the distributions of small-scale turbulence in and around the cores. Outside the core edges the turbulence structure is quite similar to that seen at $x/c = 10$. The two local maxima that sit on diagonally opposite sides of each the core are still visible, lying a little closer to the core edge than before. However, contrary to the expected decay, small-scale turbulence levels outside the cores are actually higher at $x/c = 30$ and penetrate much more deeply into the cores, substantially changing their turbulence structure. (This is in clear contrast to the single-tip vortex flow where DRLF show a factor of 9 decay in small-scale turbulence levels surrounding the core over the same streamwise distance.) Turbulence levels within the cores vary much more than at $x/c = 10$ and are considerably greater.

Further evidence for turbulence in the cores may be found in the scaling of core centre spectra. Figure 17 compares the core centre spectra measured at $x/c = 30$ with those measured at $x/c = 10$ and in the single-tip vortex flow, normalized on L_w and U_w, the lengthscales and velocity scales of the two-dimensional part of the wake far from the vortex cores. The spectra measured at $x/c = 30$ do not collapse, lying far above the other spectra. The implication is that high-frequency velocity fluctuations in the core are proportionately much larger at $x/c = 30$, consistent with the presence of new turbulence.

The change in core structure observed in the turbulence measurements appears at first sight to be at odds with the near viscous rate of decay seen in the mean tangential velocity profiles of figure 7. However, the increase in decay produced by turbulence may not be large, and we are observing it here over an uncertain distance. The data and correlations of Iversen (1976) suggest that the effective viscosity of the turbulent core would only be two to three times the kinematic viscosity at the present vortex Reynolds number.

In summary, the measurements indicate a substantial change in the turbulence structure of the vortex pair between $x/c = 10$ and 30, consistent with transition in the vortex core regions. No such change is seen in the equivalent single-vortex flow produced with one of the wings removed. Transition provides a clear physical explanation for the two stages of decay observed in the far wakes of wings (Ciffone 1974; Iversen 1976). The present experiment indicates that transition may be a consequence of short-wave instability, as is the case for vortex rings (e.g. Maxworthy 1977).

4. Conclusions

Experiments have been performed to examine the turbulence structure and development of a pair of counter-rotating wing-tip vortices. The vortices were generated by two rectangular NACA 0012 half-wings placed tip to tip, separated by 0.25 chordlengths (c). Preliminary studies showed the vortices to be insensitive to the introduction of a probe. Detailed three-component velocity measurements were made 10 and 30 chordlengths downstream of the wing leading-edges for a chord Reynolds number of 260000.

The vortices were found to be subject to small-amplitude wandering motions. At 30 chordlengths Crow instability is an important component of the wandering. At $x/c = 10$ this instability is much less dominant but the wandering motions are still symmetric about the plane of symmetry. Analysis and correction of the effects of this wandering, using the methods developed by Devenport *et al.* (1996), were necessary to reveal properly the flow structure in the vicinity of the vortex cores.

Mean velocity measurements show the overall vortex strengths to be closely matched, the cores rising but not rotating under their mutual induction. They also show the cores to be moving apart slowly from a separation of $0.45c$ at $x/c = 10$ to $0.52c$ at $x/c = 30$, roughly equal to five core diameters at both locations. The flow is rotational only in the vicinity of the cores, axial vorticity and axial velocity gradients being small elsewhere. Measurements and a potential-flow model indicate that the vortices have a total circulation equal to 60% of the bound circulation on the wings.

The turbulence structure surrounding the vortex cores is quite different at the two streamwise locations. At $x/c = 10$ the cores are embedded in an oval region of turbulence formed by the roll-up and merger of the two wing wakes. The turbulence in the rolled up sections of wake appears to be largely passive, being convected and

distorted by the mean flow, but no longer produced by it. Turbulence stresses and velocity spectra suggest the presence of large-scale turbulent eddies in the wake spirals apparently organized by mean-flow stretching. Some of the effects of stretching (e.g. increased anisotropy in the normal stresses, an intensification of velocity fluctuations at an above the passage frequency of large eddies aligned with the stretching direction) appear consistent with earlier studies of laterally stretched wakes (Keffer 1965). On the plane of symmetry between the vortices, intense vertical stretching followed by compression of the turbulence produces distinct maxima in the turbulence normal stresses perpendicular to the stretching direction, and a reversal in the sign of the turbulence production. Horizontal stretching appears important in organizing turbulent structures in the cross-flow stagnation region above the vortex pair.

At $x/c = 30$ the turbulent region surrounding the cores has grown to roughly twice the area and its structure has changed, the wake spirals having been replaced by a much more core-centred turbulence field. Remarkably, absolute turbulence levels are about the same as at $x/c = 10$. This lack of decay suggests that new turbulence is being formed, presumably through instability and roll-up in the rotational regions surrounding the cores. Although the source of the turbulence appears to be different to that at $x/c = 10$, the stretching field that appears to organize its large eddies is much the same. Consequently, velocity spectra and turbulence stresses the presence of large eddies of similar orientation. As at $x/c = 10$, stretching in between the cores produces a region dominated by vertically aligned eddies and a reversal in the turbulence production. There is also evidence of horizontally aligned structures towards the cross-flow stagnation point above the vortex pair.

The turbulence structure in the core regions, revealed by velocity spectra and high-pass filtered turbulence stress fields, also undergoes significant change. At $x/c = 10$ the cores are laminar. True turbulence levels within them are low and vary little with radius. At $x/c = 30$ the vortex cores have become turbulent. True turbulence levels within them are larger and increase rapidly with radius.

Overall, the development of the vortex pair is very different to that of the isolated vortex produced when one of the wings is removed. The core of this vortex remains laminar and the turbulence surrounding it dies away rapidly with downstream distance. We conclude, therefore, that it is the interaction between the counter-rotating vortices that stimulates transition in their cores and that maintains the intensity of the turbulent field that surrounds them. Core spectral measurements suggest that transition may be a result of short-wave instability, as is the case for vortex rings. Similar transition of the cores may be responsible for the two stages of vortex decay seen by previous authors studying the far wakes of lifting wings.

The experimental data presented in this paper may be accessed on the World Wide Web at *http:/www.aoe.vt.edu/flowdata.html*.

The authors would like to thank Mike Rife and Gautam Sharma for their assistance in taking many of the above measurements. The financial support of ARPA, administered by Mr Gary W. Jones and the office of naval Research, through ONR contracts N00014-90-J-1909 and N00014-91-J-1773 is also gratefully acknowledged.

REFERENCES

Baldwin, B. S., Chigier, N. A. & Sheaffer, Y. S. 1973 Decay of far-flowfield in trailing vortices. *AIAA J.* **11**, 1601–1602.

Barkey Wolf, F. D. 1987 Swept and unswept separation bubbles. PhD dissertation, University of Cambridge.

Betz, D. 1933 Behavior of vortex systems. *NACA TM* 713.

Burnham, D. C., Sullivan, T. E. & Wilk, L. S. 1976 Measurement of wake vortex strength by means of acoustic back scattering. *J. Aircraft* **13**, 889–894.

Chevalier, H. 1973 Flight test studies of the formation and dissipation of trailing vortices. *J. Aircraft* **10**, 14–18.

Ciffone, D. L. 1974 Correlation for estimating vortex rotational velocity downstream dependence. *J. Aircraft* **11**, 716–717.

Ciffone, D. L. & Orloff, K. L. 1974 Axial flow measurements in trailing vortices. *AIAA J.* **12**, 1154–1155.

Ciffone, D. L. & Orloff, K. L. 1975 Far-field wake-vortex characteristics of wings. *J. Aircraft* **12**, 464–470.

Ciffone, D. L. & Orloff, K. L. 1976 Application of laser velocimetry to aircraft wake vortex measurements. *Wake Vortex Minimization*, *NASA SP* 409, pp. 157–192.

Corsiglia, V. R., Schwind, R. G. & Chigier, N. A. 1973 Rapid scanning, three-dimensional hot-wire anemometer surveys of wing-tip vortices. *J. Aircraft* **10**, 752–757.

Crow, S. C. 1970 Stability theory for a pair of trailing vortices. *AIAA J.* **8**, 2172–2179.

Devenport, W. J., Rife, M. C., Liapis, S. I. & Follin, G. J. 1996 The structure and development of a wing-tip vortex. *J. Fluid Mech.* **312**, 67–106.

Didden, N. 1977 *Mitt. Max-Planck-Inst. Strömungsforsch. Aerodyn. Versuchsanst.*, no. 64. (See alternatively: Van Dyke, M. 1982 *An Album of Fluid Motion*, pp. 66, Parabolic Press, Stanford, CA.)

Donaldson, C. duP. 1972 Calculation of turbulent shear flows for atmospheric and vortex motions. *AIAA J.* **10**, 4–12.

Eliason, B. G., Gartshore, I. S. & Parkinson, G. V. 1975 Wind tunnel investigation of Crow instability. *J. Aircraft* **12**, 985–988.

El-Ramly, Z. & Rainbird, W. J. 1977 Flow survey of the vortex wake behind wings. *J. Aircraft* **14**, 1102–1108.

Follin, G. J. 1996 The turbulence structure of trailing vortex wakes. MS thesis, Dept of Aerospace and Ocean Engineering, Virginia Polytechnic Institute and State University.

Garodz, L. J., 1971 Federal Aviation Administration full-scale aircraft vortex wake turbulence flight test investigations: past, present, and future. *AIAA 9th Aerospace Sciences Meeting*, *New York*, *NY*, *25–27 January*, *1971*; *AIAA Paper*-71-97.

Iversen, J. D. 1976 Correlation of turbulent trailing vortex decay data. *J. Aircraft* **13**, 338–342.

Keffer, J. F. 1965 The uniform distortion of a turbulent woke. *J. Fluid Mech.* **22**, 135–159.

Liu, H.-T. 1992 Effects of ambient turbulence on the decay of a trailing vortex wake. *J. Aircraft* **29**, 255–263.

Locke, C. A., Hirsa, A. & Rubin, M. D. 1993 Short-wave instability on a laminar vortex pair. *ASME Forum on Unsteady Flows*, **FED 157**, 73–81.

McCormick, B. W., Tangler, J. L. & Sherrieb, H. E. 1968 Structure of trailing vortices. *J. Aircraft* **5**, 260–267.

Maxworthy, T. 1972 The structure and stability of vortex rings. *J. Fluid Mech.* **51**, 15–32.

Maxworthy, T. 1974 Turbulent vortex rings. *J. Fluid Mech.* **64**, 227–239.

Maxworthy, T. 1977 Some experimental studies of vortex rings. *J. Fluid Mech.* **81**, 465–495.

Melander, M. V. & Hussain, F. 1991 Coherent structure dynamics: Interaction between large and fine scales. *8th Symp. of Turbulent Shear Flows*, *Technical University of Munich 9–11 September*.

Miller, G. D. & Williamson, C. H. K. 1995 Turbulence structures in the trailing vortex wake of a delta wing. *10th Symp. on Turbulent Shear Flows*, *Pennsylvania State University*, *14–16 August*.

Sarpkaya, T. 1983 Trailing vortices in homogeneous and density-stratified media. *J. Fluid Mech.* **136**, 85–109.

Sarpkaya, T. & Daly, J. J. 1987 Effect of ambient turbulence on trailing vortices. *J. Aircraft* **26**, 399–404.

Scorer, R. S. & Davenport, L. J. 1970 Contrails and aircraft downwash. *J. Fluid Mech.* **43**, 451–464.

Sullivan, J. P., Widnall, S. E. & Ezekiel, S. 1973 Study of vortex rings using a laser Doppler velocimeter. *AIAA J.* **11**, 1384–1389.

Thomas, P. J. & Auerbach, D. 1994 The observation of the simultaneous development of a long- and a short-wave instability mode on a vortex pair. *J. Fluid Mech.* **256**, 289–302.

Tombach, I. 1973 Observations of atmospheric effects on vortex wake behavior. *J. Aircraft*, **10**, 641–647.

Widnall, S. E., Bliss, D. B. & Tsai, C. 1974 The instability of short waves on a vortex ring. *J. Fluid Mech.* **66**, 35–47.

Wilson, D. J., Zalay, A. D., Brashears, M. R., Craven, C. E., Shrider, K. R. & Jordan, A. J. 1979 Full-scale wake flow measurements with a mobile laser Doppler velocimeter. *J. Aircraft* **16**, 155–161.